EM-Neuro Modeling Across Scales for Bioelectronic Medicine

Lecture 9: Recording Modalities, Signal Content & the Reciprocity Theorem

Esra Neufeld[*] and Taylor Newton[*†]

[*]IT'IS Foundation for Research on Information Technologies in Society

[†]Integrated Systems Laboratory, ETH Zurich

Outline for Today

- Extracellular Potentials at the Source — MUA, LFP, CSD
- Scalp-Level Signals — EEG, MEG, electrode layouts, reference problem
- The EEG Forward Problem — Poisson BVP, lead-field matrix, tissue conductivities
- The Reciprocity Theorem — Helmholtz 1853 → modern lead-field theory → tES
- Other Recording Modalities — fMRI/BOLD and eCAPs
- Engagement Metrics & Summary — Exposure vs. response, pivot to W10
- Exercise Preview — Mini project work

Course Outline

DATE	LECTURE THEME
19.02	Motivation, logistics & tooling (EN, TNE)
26.02	Ion channels & membranes (EN)
05.03	Axon models, activating functions & electrical stimulation (EN)
12.03	EM field simulation fundamentals & coupled EM-neuro workflows (EN)
19.03	Peripheral nerves & interfaces for bioelectronic medicine (EN)
26.03	Spinal cord stimulation for neuroprosthetics and pain management & low-frequency exposure safety (TNE)
02.04	Morphology, synapses, microcircuits; point vs spiking networks (TNE)
09.04	No class: Easter break
16.04	Neural mass & whole brain models; hybridization (TNE)
23.04	Recording modalities, signal content & the reciprocity theorem (TNE)
30.04	Non invasive brain stimulation & temporal interference (TNE)
07.05	Image based/personalized treatment planning and optimization (EN)
14.05	No class: Ascension Day
21.05	Verification, validation, UQ, and reproducibility (EN)
28.05	Project presentations & synthesis (EN, TNE)

Room: ETZ E7

13:15-14:00 Lecture

14:00-14:15 Break

14:15-15:00 Lecture

14:00-14:15 Break

15:15-16:00 Exercise

Recorded Lectures & Course Material

Provided Here

Exercise Outline

DATE	EXERCISE THEME
19.02	"Hello Neuron": integrate-and-fire in Python/NEURON
26.02	Point neuron phase portrait; basic time integration numerics
05.03	Recruitment prediction for myelinated axon using AF/GAF
12.03	EM (FEM) modeling of transcranial brain stimulation
19.03	Stimulation selectivity and signal content modeling for nerve interfaces
26.03	Mini project work
02.04	Mini project work
09.04	No class: Easter break
16.04	Guest (Neuromodulation Spin-Off – Z43)
23.04	Mini project work
30.04	Guest (NIBS – Kinderspital)
07.05	Guest (SCS – UNIL)
14.05	No class: Ascension Day
21.05	Mini project work
28.05	Project presentations

Room: ETZ E7

13:15-14:00 Lecture

14:00-14:15 Break

14:15-15:00 Lecture

14:00-14:15 Break

15:15-16:00 Exercise

Learning Objectives

- Derive the extracellular potential produced by a multi-compartment neuron from transmembrane currents; distinguish point-source and line-source approximations [1, 2]
- Distinguish MUA and LFP by frequency content, spatial reach, and biophysical origin [3, 6, 7]
- Explain why cortical pyramidal cells dominate scalp EEG/MEG via open-field geometry; quantify per-neuron and population current dipole moments [8, 18, 19]
- Write down quasi-static Poisson volume-conductor equation and the lead-field matrix formulation $\mathbf{V} = \mathbf{LJ}$ [32, 33]
- State and interpret the Helmholtz–Plonsey reciprocity theorem [47, 48, 50]
- Use reciprocity to connect the EEG forward problem to the tES forward problem, and explain the dot-product intuition for montage design [53, 54, 55]
- Describe biophysical chain linking neural activity to BOLD via the Balloon–Windkessel model [59, 61, 62]
- Differentiate exposure-based metrics (|E|, SAR, VTA) from response-based metrics (EEG, BOLD, eCAP) and explain why closed-loop control requires the latter [68, 69, 70]

Recommended Reading

- Halnes G, Ness TV, Næss S, Hagen E, Pettersen KH, Einevoll GT. *Electric Brain Signals: Foundations and Applications of Biophysical Modeling*. Cambridge University Press; 2024.
- Buzsáki, G., Anastassiou, C.A. & Koch, C. (2012). The origin of extracellular fields and currents — EEG, ECoG, LFP and spikes. Nat. Rev. Neurosci. 13:407–420 [2]
- Hallez, H. et al. (2007). Review on solving the forward problem in EEG source analysis. J. NeuroEng. Rehabil. 4:46 [32]
- Hämäläinen, M., Hari, R., Ilmoniemi, R.J., Knuutila, J. & Lounasmaa, O.V. (1993). Magnetoencephalography — theory, instrumentation, and applications. Rev. Mod. Phys. 65:413–497 [21]
- Rush, S. & Driscoll, D.A. (1969). EEG electrode sensitivity — an application of reciprocity. IEEE Trans. Biomed. Eng. BME-16:15–22 [22]
- Logothetis, N.K. (2008). What we can do and what we cannot do with fMRI. Nature 453:869–878 [62]

Outline for Today

- **Extracellular Potentials at the Source — MUA, LFP, CSD**
- Scalp-Level Signals — EEG, MEG, electrode layouts, reference problem
- The EEG Forward Problem — Poisson BVP, lead-field matrix, tissue conductivities
- The Reciprocity Theorem — Helmholtz 1853 → modern lead-field theory → tES
- Other Recording Modalities — fMRI/BOLD and eCAPs
- Engagement Metrics & Summary — Exposure vs. response, pivot to W10
- Exercise Preview — Mini project work

Neuroimaging Spatiotemporal Resolution (W02)

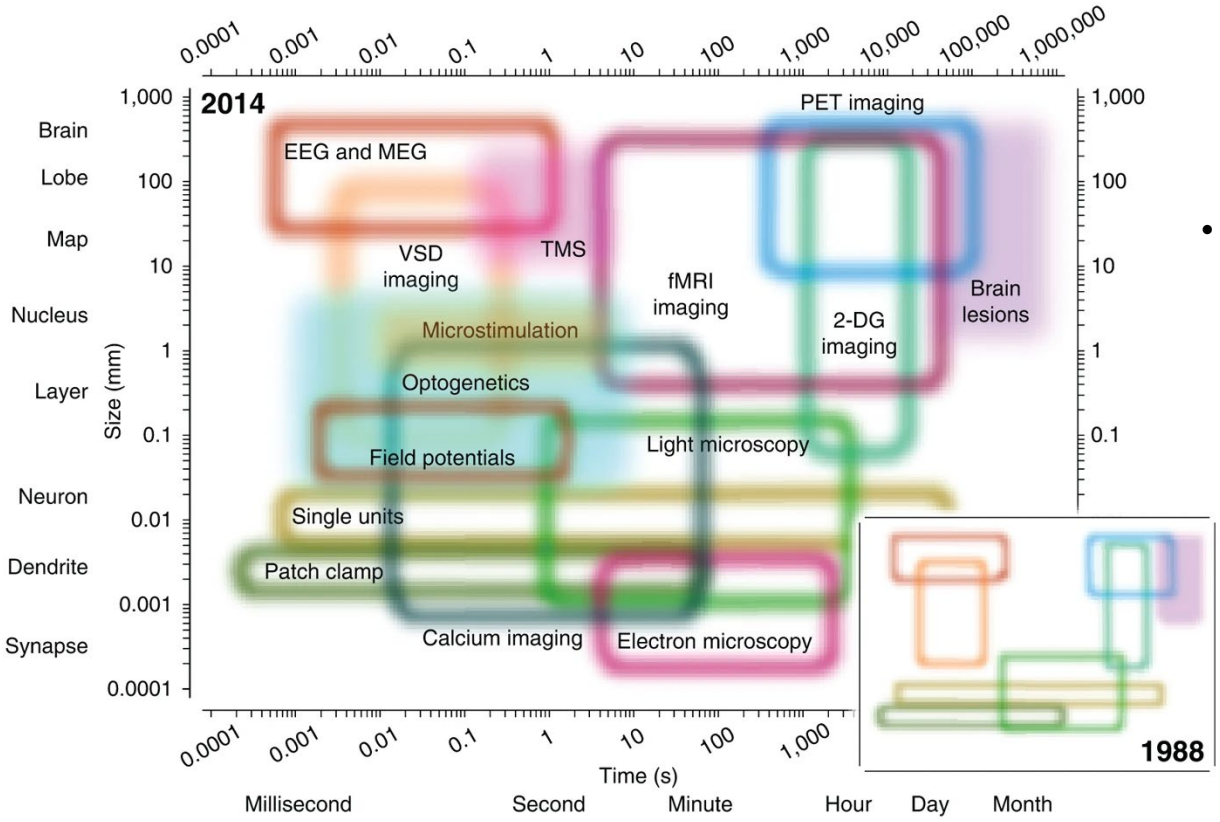

- Every technique trades spatial resolution for temporal coverage, or vice versa: No single modality spans the full range from synapse to brain, millisecond to month

- Electrocorticography (ECoG) and field potentials occupy the intermediate "meso-scale" — the target zone for most bioelectronic devices in this course
- Since 1988: The landscape has expanded dramatically — optogenetics, calcium imaging, Neuropixels, and functional MRI (fMRI) have filled gaps that did not exist in the original diagram

Image: J. M. Bower and D. Beeman, *The Book of GENESIS: Exploring Realistic Neural Models with the GEneral NEural SImulation System*, 2nd ed. New York: Springer, 1998.

Source Currents from the Cable Equation

- **Before we can sum the transmembrane currents $I_{m,k}$ at a distant electrode (next slide), we need to know what drives them.** McNeal [77] derives them from the discretized cable equation; under his assumptions (see footnote*), the nodal dynamics reduce to:

$$\frac{dV_n^m}{dt} = \left[-i_{ion,n} + \frac{d\,\Delta x}{4\rho_i \ell}\left(\frac{V_{n-1}^m - 2V_n^m + V_{n+1}^m}{\Delta x^2} + \frac{V_{n-1}^e - 2V_n^e + V_{n+1}^e}{\Delta x^2}\right)\right]/c$$

source currents

$\propto$ activating function (AF)

- **Two second-differences, added.** The axial current through R_i (axial resistance) depends on $V_i = V^m + V^e$ so Kirchhoff at node n gives a curvature in each component. The continuous cable equation is recovered in the $\Delta x \to 0$ limit.
- **Recording (no applied field, $V^e \approx 0$ along neurite):**
  - Second term vanishes $\rightarrow I_{m,n}$ set by the *intrinsic* V^mcurvature alone
  - These $I_{m,n}$ are precisely the source currents populating sum on the next slide
- **Stimulation (W05 callback; applied $V^e(s,t)$ from external electrodes):**
  - First term is the membrane response to be solved for; second term is the imposed drive $\rightarrow AF_n \propto (V_{n-1}^e - 2V_n^e + V_{n+1}^e)/\Delta x^2$
  - Depolarizes V^m where the applied V^e has large curvature — ignites channel gating if threshold reached
- **Takeaway:** Recording and stimulation are the two natural limits — which term is driver and which is response depends on whether an external field is applied.

*McNeal [77] assumes a long myelinated fiber and an ideal passive internode (zero leak, zero capacitance — current flows axially through axoplasm and transmembrane only at nodes), and lumped nodal membrane dynamics.

V^m, V^e = intra/extracellular potentials at node n; $i_{ion,n}$= ionic current; d = axon diameter; Δx = node-to-node dist.; ρ_i = axial resistivity; ℓ = node length; c = specific membrane capacitance.

Recordings ≈ Weighted Sum of Transmembrane Currents

σ = medium conductivity; r = field point; r_k = k-th compartment centre; $I_{m,k}$ = its transmembrane current; Δs_k = its length; h_k, l_k = signed distances from r's foot on the compartment axis to the two endpoints; $r_{\perp,k}$ = perpendicular distance from r to that axis; N = number of compartments.

- Quasi-static, ohmic, **infinite homogeneous, isotropic medium** with constant σ → V_e = linear sum of transmembrane currents over compartments r_k [1, 2]:

$$V_e(\mathbf{r},t) = \frac{1}{4\pi\sigma}\sum_{k=1}^{N}\frac{I_{m,k}(t)}{\|\mathbf{r}-\mathbf{r_k}\|} \quad \text{(point−source)}$$

Line-source approximation: assume cylindrical compartments of length Δs_k [1]:

$$V_e(\mathbf{r},t) = \frac{1}{4\pi\sigma}\sum_{k}\frac{I_{m,k}(t)}{\Delta s_k}\ln\left|\frac{\sqrt{h_k^2+r_{\perp,k}^2}-h_k}{\sqrt{l_k^2+r_{\perp,k}^2}-l_k}\right|$$

  - ⟹ for *realistic tissue*, factor $1/(4\pi\sigma|\boldsymbol{r}-\boldsymbol{r}_k|)$ replaced by head-model Green's function $\mathrm{G}(\mathbf{r},\mathbf{r}_k)$ computed numerically—boundary element method (BEM)/finite element method (FEM); the linear-sum structure is preserved.
  - Accurate to few % except within ~1 μm of segment
- Kirchhoff current conservation, isolated neuron: $\Sigma_k I_{m,k}(t) = 0$ — physical requirement; leading-order far field → dipolar, not monopolar

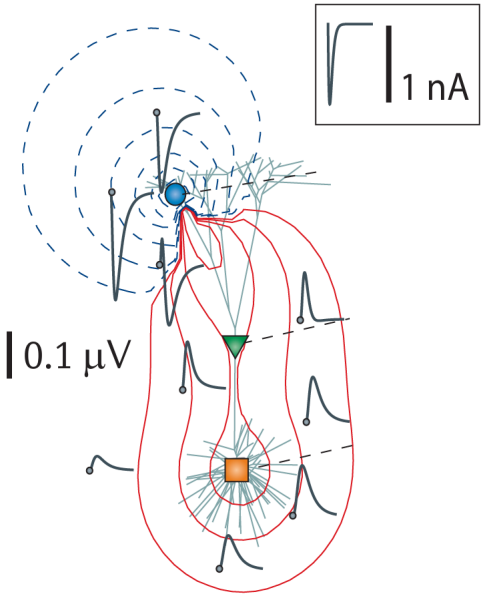

Simulated local field potential (LFP) traces (left panel; grey) in response to an excitatory synaptic current input (a sink, shown by the blue circle).

Buzsáki, G., Anastassiou, C. & Koch, C. *Nat Rev Neurosci* 13, 407–420 (2012)

Multi-Unit Activity (MUA): Spikes, Sorting, Ensembles

- Spectral: extracellular spike power 300 Hz – 5 kHz → high-pass ~300–500 Hz isolates MUA [2]
- Detection geometry (Buzsáki 2004, Henze 2000) [3, 4]:
  - Cylinder ~140 µm radius (~1000 neurons) around silicon-probe site, rat cortex
  - small minority reliably separable w/ current probes + spike-sorting
  - Single-unit amplitudes largest within ~50 µm of soma (Henze 2000)

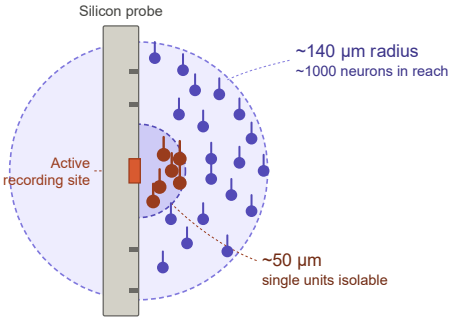

- Robust amplitude threshold (Quian Quiroga 2004, wave_clus) [5]:

$$\mathrm{Thr} = 4\sigma_n, \qquad \sigma_n = \mathrm{median}(|x|)/0.6745 \quad \text{(estimates "noise" SD)}$$

  - median absolute deviation (MAD) estimator robust to spikes
- Application: intracortical brain machine interfaces (BMIs) (BrainGate, Utah array); single-unit encoding, ensemble decoding

x = band-passed signal

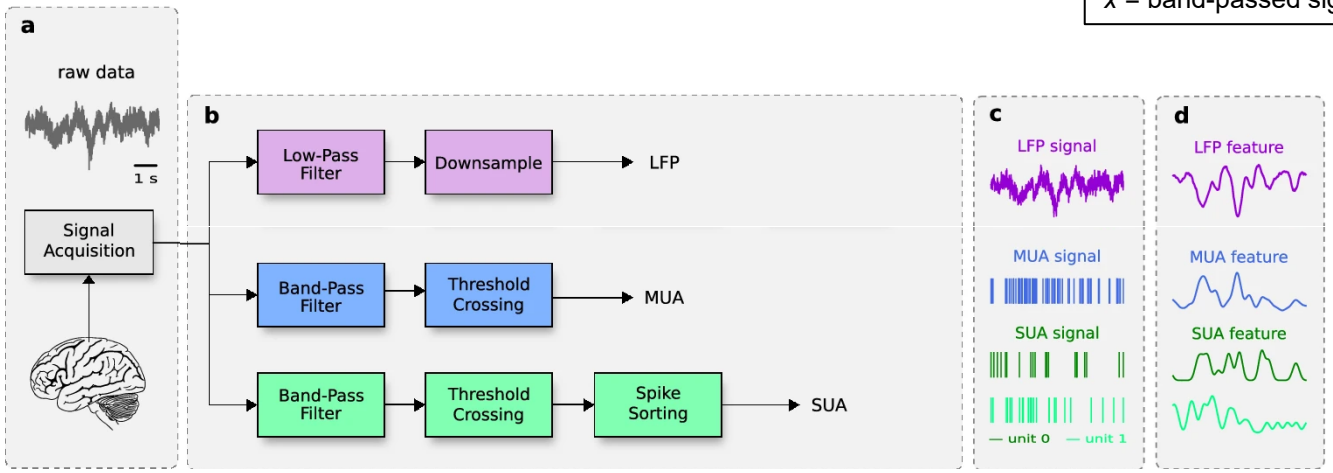

Multi-Unit Activity (MUA): Spikes, Sorting, Ensembles

- Spectral: extracellular spike power 300 Hz – 5 kHz → high-pass ~300–500 Hz isolates MUA [2]
- Detection geometry (Buzsáki 2004, Henze 2000) [3, 4]:
  - Cylinder ~140 µm radius (~1000 neurons) around silicon-probe site, rat cortex
  - small minority reliably separable w/ current probes + spike-sorting
  - Single-unit amplitudes largest within ~50 µm of soma (Henze 2000)

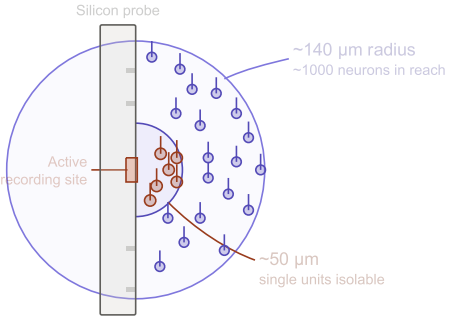

- Robust amplitude threshold (Quian Quiroga 2004, wave_clus) [5]:

$$\mathrm{Thr} = 4\sigma_n, \qquad \sigma_n = \mathrm{median}(|x|)/0.6745 \quad \text{(estimates "noise" SD)}$$

  - median absolute deviation (MAD) estimator robust to spikes
- Application: intracortical brain machine interfaces (BMIs) (BrainGate, **Utah array**); single-unit encoding, ensemble decoding

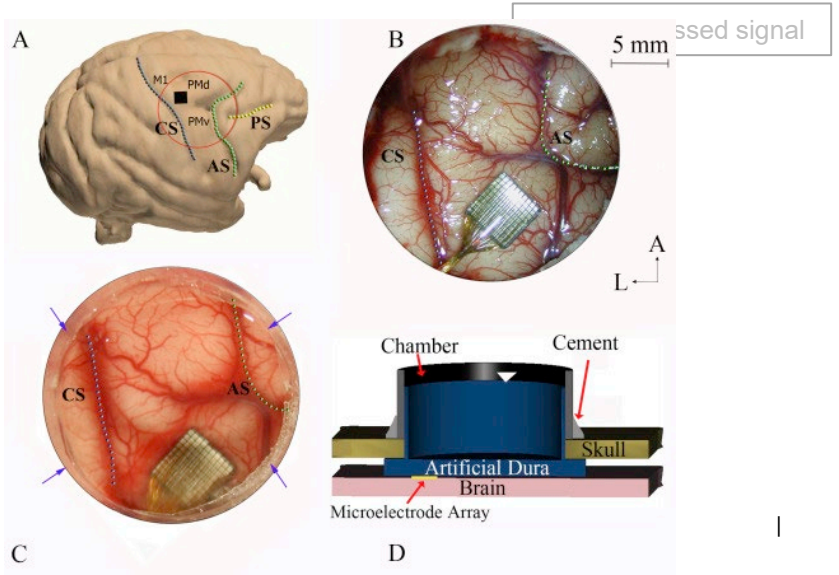

M. M. Chernov et al., *J. Neurosci. Methods*, vol. 263, pp. 7–14, Apr. 2016

Local Field Potential (LFP): Synaptic, Slow, Spatially Extended

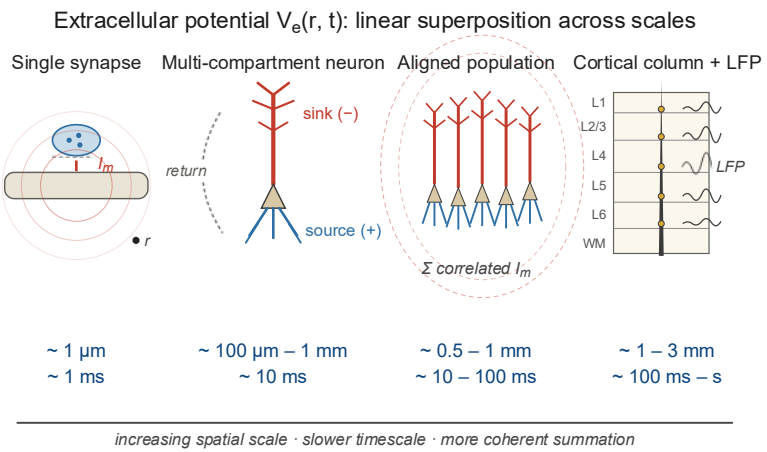

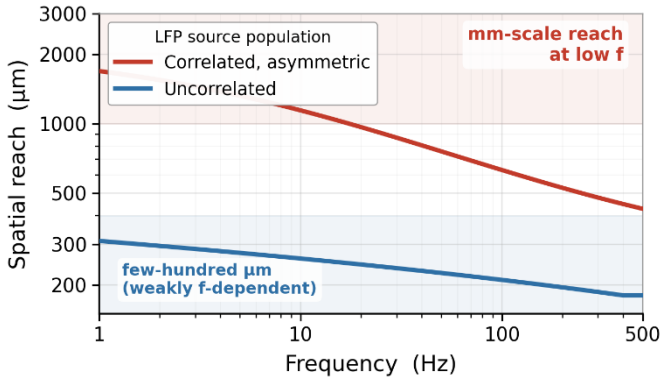

- Spectral: low-pass ~300 Hz (some to 500); ~1/f power spectrum [6]
- Dominated by synaptic transmembrane currents, not action potentials (APs) [2, 6]:
  - Synaptic timescales (ms–tens of ms) >> spike duration (~1 ms) → temporal overlap → coherent sum
  - Extracellular spike waveform is biphasic (≈zero-mean by charge conservation) + asynchronous firing → destructive interference at distance
  - Synchronized spike volleys → high-frequency LFP contribution possible
- Spatial reach depends on frequency + correlation structure (Łęski 2013) [7]:
  - Uncorrelated input: reach weakly freq-dependent, ~few hundred µm
  - Correlated input + asymmetric dendritic targeting (apical- or basal-only): low-freq (<10 Hz) power dominates by ≥1 order of magnitude; reach → mms
- LFP ≠ 'local' in naive sense — interpretation requires input correlation structure

Geometry Determines the Far Field (EEG/MEG)

- Macroscopic $V_e \propto$ geometric alignment of transmembrane currents, not just amplitude [8]
- Pyramidal cells — aligned in palisades, long apical dendrites:
  - Dipole-like open fields
  - Contributions sum coherently at distance
  - Dominate scalp EEG and magnetoencephalography (MEG)
- Radially symmetric neurons — stellate, granule, spherico-radial motoneurons:
  - Sinks/sources very close to each other and cancel at cell length scale
  - Randomly oriented
  - Closed fields → negligible far-field LFP + scalp EEG
  - May still contribute locally to intracranial fields
- Scalp EEG dominated by synchronously active, aligned cortical pyramidal postsynaptic potentials (PSPs) — one of three requirements (alignment, synchrony, extent) for scalp-visible signal [2, 17]

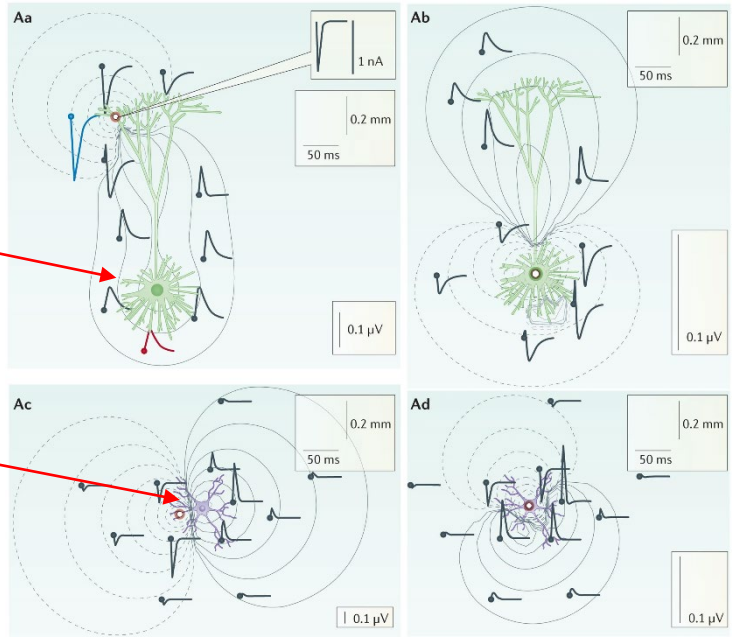

Einevoll, G. *et al. Nat Rev Neurosci* **14**, 770–785 (2013).

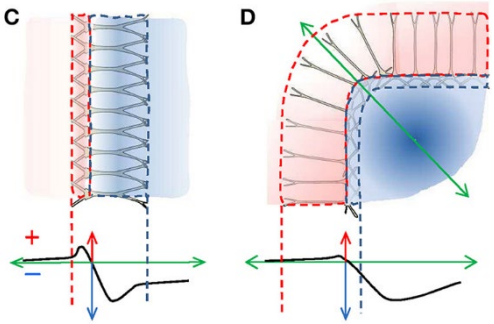

Herreras O Front. Neural Circuits (2016) 10:101.

Current Source Density: Inverting the Forward Map

- **LFP** = measured, volume-conducted — one contact sees every current in its reach.
- **current source density (CSD)** = derived, local — net transmembrane current density (sink or source) at a location.
- ∇·J (current density J = −σ∇V) in quasi-static ohmic medium → CSD:

  $$C(\mathbf{r},t) \equiv -\nabla \cdot [\sigma(\mathbf{r})\nabla V(\mathbf{r},t)]$$

  - C > 0 = source (outward transmembrane current); C < 0 = sink
- 1-D laminar estimator (linear probe, spacing h):

  $$\hat{C}(z_i,t) \approx -\sigma \frac{V(z_{i+1}) - 2V(z_i) + V(z_{i-1})}{h^2}$$

  N.B. above assumes **σ constant along *z* & sources constant *in plane*** ⟹ only $\partial^2V/\partial z^2$ survives; inverse/kernel CSD (iCSD/kCSD) relax both by modelling the source geometry + σ profile explicitly

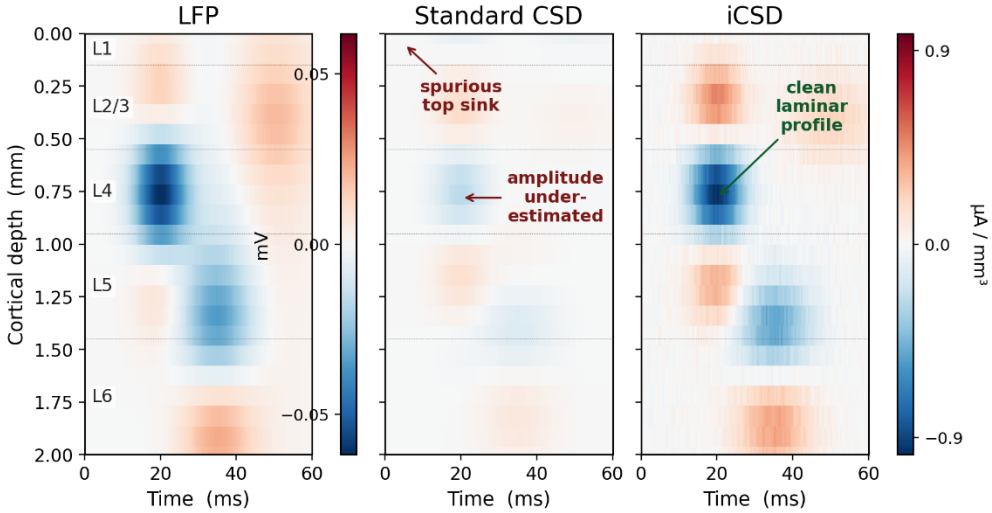

- Lineage: classical CSD [9, 10] → iCSD (parametric forward inversion) [11, 12] → kCSD (non-parametric kernel, arbitrary electrode geometry) [13]

probe contact spacing *h*; depth coordinate *z*

Outline for Today

- Extracellular Potentials at the Source — MUA, LFP, CSD
- **Scalp-Level Signals — EEG, MEG, electrode layouts, reference problem**
- The EEG Forward Problem — Poisson BVP, lead-field matrix, tissue conductivities
- The Reciprocity Theorem — Helmholtz 1853 → modern lead-field theory → tES
- Other Recording Modalities — fMRI/BOLD and eCAPs
- Engagement Metrics & Summary — Exposure vs. response, pivot to W10
- Exercise Preview — Mini project work

Berger 1929: "Elektrenkephalogramm des Menschen"

- Berger (Jena Hospital): first systematic non-invasive human EEG [16]
  - Siemens double-coil string galvanometer; needle/plate electrodes
  - Named α rhythm (8–13 Hz, posterior, eyes-closed) & β rhythm (13–30 Hz, frontal, alert/active)
  - Scalp amplitudes ~50–100 μV reported — matches modern values
- Pre-Berger (invasive animal):
  - Caton 1875 — first cortical potentials in rabbit/monkey
  - Pravdich-Neminsky 1912 — first animal EEG
- Berger's contribution = non-invasive human measurement → EEG becomes a clinical & scientific modality

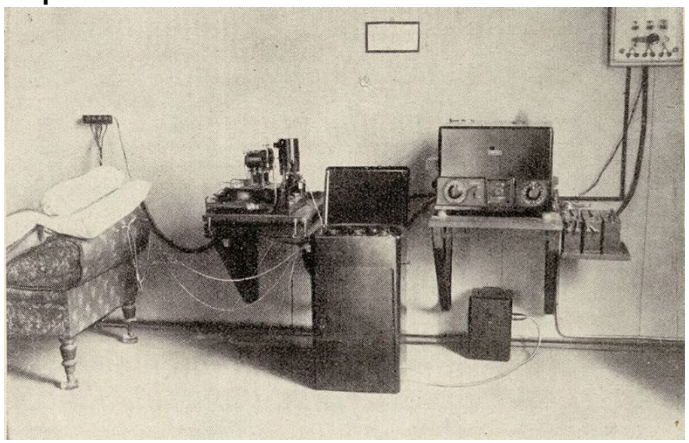

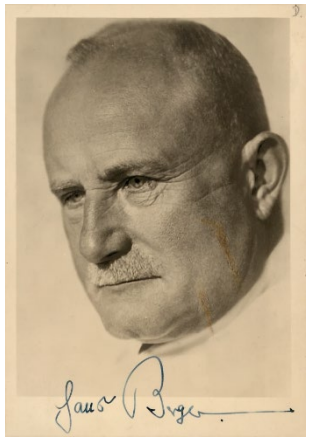

Lemke et al., *Clin Epileptol* **37** (Suppl 3), 112–119 (2024).

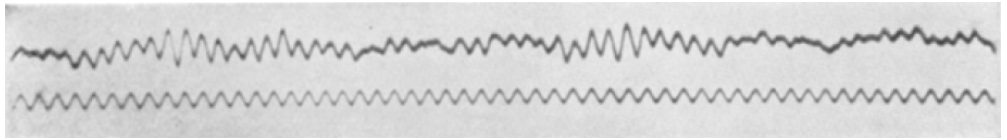

Berger H. *Electroencephalogr Clin Neurophysiol*. 1969;Suppl 28:37-73.

Three Ingredients for Scalp EEG

- **Alignment**: L2/3 + L5 pyramidal cells have 1–2 mm apical dendrites ⊥ cortex → equivalent dipole normal to cortex [2, 8]
- **Synchrony**: excitatory/inhibitory PSPs last 10–250 ms → coherent sum; spikes (~1 ms) too brief + typically desynchronous → no scalp sum [2]
- **Extent**: min synchronous cortical area for scalp-visible signal w/o averaging ≈ 6 cm² (Nunez & Srinivasan 2006) [17]
- Per-neuron current dipole moment (Murakami & Okada 2006, 2015) [18, 19]:

Component	Magnitude	Cell class
Spike transients (bipolar, limited sum)	up to ~3 pA·m	L5 pyramidal
Burst/envelope (slow, EEG-relevant)	0.29 pA·m	L2/3 pyramidal
Burst/envelope (slow)	0.41–0.90 pA·m	L5 pyramidal
Burst/envelope (slow)	0.17–0.20 pA·m	CA1/CA3

- Population dipole-moment density, for a *coherently activated, approximately planar patch with uniformly oriented dipoles*: $q \equiv |\mathbf{Q_{pop}}|/A \lesssim$ 1–2 nAm/mm² — physiological upper range, not universal constant.

$$\mathbf{Q_{cell}} = \int_{V_{cell}} \mathbf{J^p}\, dV \approx I\mathbf{d} \qquad \mathbf{Q_{pop}} = \sum_{i=1}^{N} \mathbf{Q_{cell,i}} \qquad q = |\mathbf{Q_{pop}}|/A$$

Sanity check: 1 nAm/mm² × 600 mm² ≈ 600 nAm → ~10–50 µV scalp — matches Berger

$\mathbf{J^p}$ is the "impressed"/"source" current; generated by neural biophysics, not driven by local E-field (via $\sigma \mathbf{E}$). Current-dipole moment Q_{cell} (integral of impressed current density p over cell volume V_{cell}); far-field equivalent I*d, with transmembrane current I, dipole separation d; population-density $q = Q_{pop}$ / cortical area A.

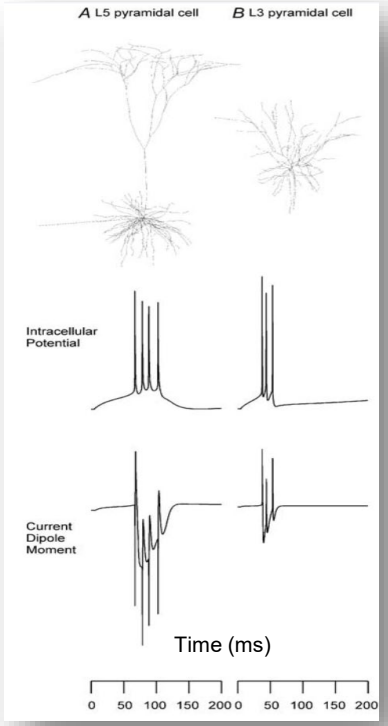

Murakami, S. and Okada, Y. *J. Physiol.* (2006) 575: 925-936.

The Current Dipole: From Cell to Far Field

- Two opposite point currents ±I separated by d in infinite homogeneous medium (cond. σ), far field ($|\mathbf{r} - \mathbf{r_0}| >> d$):

$$\Phi(\mathbf{r}) \approx \frac{1}{4\pi\sigma} \frac{\mathbf{Q} \cdot (\mathbf{r} - \mathbf{r_0})}{|\mathbf{r} - \mathbf{r_0}|^3}, \quad \mathbf{Q} \equiv I\mathbf{d}$$

- Generalized (any "impressed"—i.e., neural source—current density $\mathbf{J^p}$ confined to V_0):

$$\mathbf{Q} = \int_{V_0} \mathbf{J^p}(\mathbf{r}')dV'$$

  - Zeroth multipole vanishes by current conservation (slide 8)
  - Q = first non-zero multipole (Sarvas 1987 Eq. 16) [20]

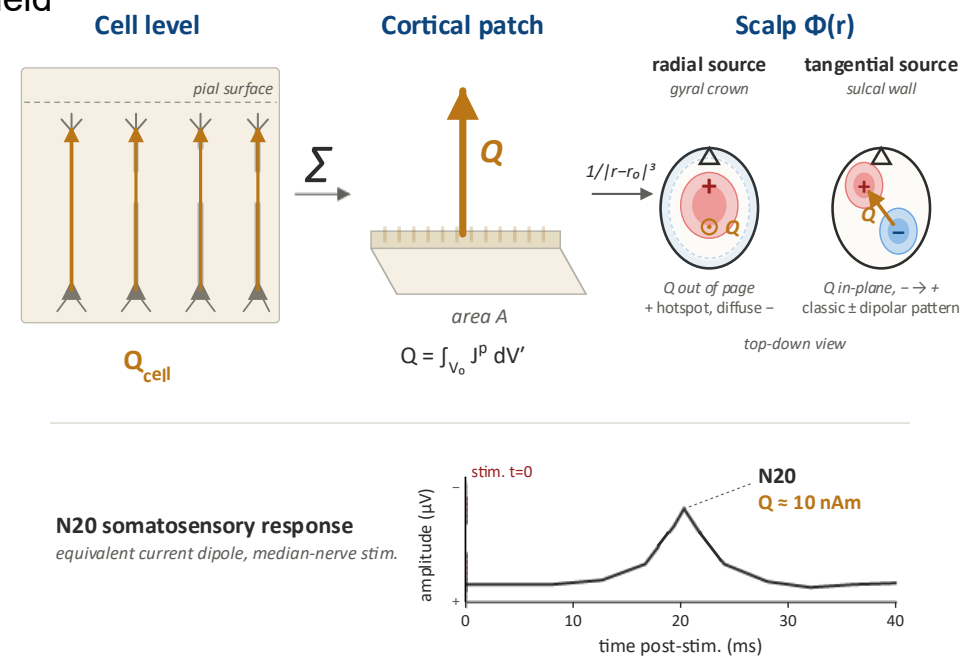

- Equivalent-current-dipole magnitudes for evoked responses — pedagogical values, not invariant constants:
  - N20 (negative-going ≈20 ms median-nerve somatosensory response): Q ≈ 10 nAm
  - Epileptic spike: Q ≈ 100 nAm
- Bridge → Part III: forward map from Q (or dipole distribution) to scalp voltages via realistic head anatomy

Biot–Savart, Sarvas: Why MEG Sees Sulcal Walls

- Magnetoencephalography (**MEG**): non-invasive recording of the weak magnetic fields produced by neural currents — magnetic counterpart to EEG
- Biot–Savart, quasi-static limit. **B** = magnetic flux density; superconducting quantum interference device (SQUID) sensors measure the component normal to scalp:

$$\mathbf{B}(\mathbf{r}) = \frac{\mu_0}{4\pi} \int \frac{\mathbf{J}(\mathbf{r}') \times (\mathbf{r} - \mathbf{r}')}{|\mathbf{r} - \mathbf{r}'|^3} dV'$$

- Sarvas 1987 [20] closed form for a spherically symmetric conductor with dipole **Q** at $\mathbf{r_0}$: $\mathbf{B}(\mathbf{r})$ (outside conductor) $\propto \mathbf{Q} \times \mathbf{r_0}$, up to scalars.
- *Radial insensitivity — key physical constraint:*
  - Idealized case: **Q** ∥ $\mathbf{r_0}$ (radial) → **Q** × $\mathbf{r_0}$ = 0 → **B** = 0 exactly outside [20]
  - But real cortex is folded: gyral crown (sheet ∥ skull) → dipole radial → **MEG blind.** sulcal wall (sheet ⊥ skull) → dipole tangential → **MEG visible**
  - Tangential/radial sensitivity ~5–10:1 [21]

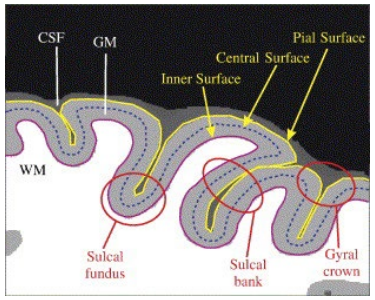

- Resolution [21]: spatial 2–3 mm, temporal <1 ms
- **MEG**: clean tangential sulcal sources; **EEG**: sees both but skull-smeared. Joint EEG+MEG fusion standard (Baillet 2017) [27]

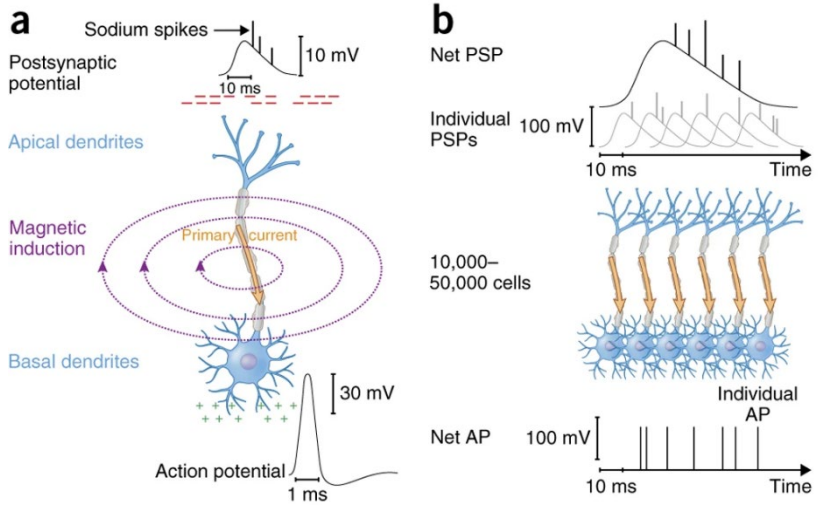

Baillet, S. *Nat Neurosci* **20**, 327–339 (2017).

D. Tosun et al., *NeuroImage*, vol. 29, no. 3, pp. 838–852, Feb. 2006

Electrode Placement and the Reference Problem

- Electrode layout hierarchies (*10-X: inter-electrode distance of X% skull circumference*):
  - **10–20** (Jasper 1958) [28]: 19 positions, ~6 cm spacing — clinical standard
  - **10–10** (Klem 1999) [29]: ~74 positions, ~3 cm spacing; adds AF/FC/CP/PO* rows
  - **10–5** (Oostenveld & Praamstra 2001) [30]: up to 345 positions, ~1.5 cm — required for surface-Laplacian / high-res EEG

- Reference problem — EEG = potential difference; no 'true ground' in head:
  - Single physical ref (Cz, nose, mastoid): contaminates all channels w/ ref-site activity
  - Linked mastoids: biases toward central midline; links hemispheres electrically
  - Common average reference (CAR): unbiased in dense-coverage limit (*N* electrodes)

$$\Phi_i^{\mathrm{CAR}}(t) = \Phi_i(t) - \frac{1}{N}\sum_{j=1}^{N}\Phi_j(t)$$

- Reference electrode standardization technique (REST) (Yao 2001) [31]: model-based analytical ref at infinity; accuracy bounded by head model
  - Surface Laplacian / CSD: reference-free; needs ≥ 10–10

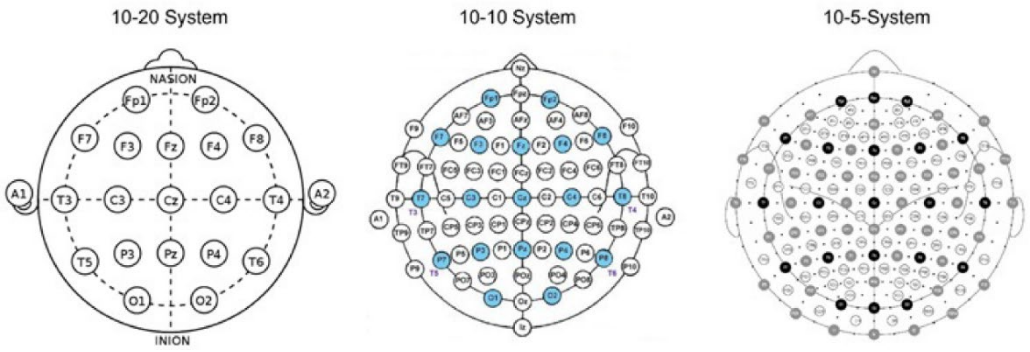

*anterior-frontal, fronto-central, centro-parietal, parieto-occipital

Mihai, A.S. et al., *Sensors* **2025**, *25*, 3321.

Electrode Placement and the Reference Problem

- Electrode layout hierarchies (*10-X: inter-electrode distance of X% skull circumference*):
  - **10–20** (Jasper 1958) [28]: 19 positions, ~6 cm spacing — clinical standard
  - **10–10** (Klem 1999, IFCN) [29]: ~74 positions, ~3 cm spacing; adds AF/FC/CP/PO rows
  - **10–5** (Oostenveld & Praamstra 2001) [30]: up to 345 positions, ~1.5 cm — required for surface-Laplacian / high-res EEG

- Reference problem — EEG = potential difference; no 'true ground' in head:
  - Single physical ref (Cz, nose, mastoid): contaminates all channels w/ ref-site activity
  - Linked mastoids: biases toward central midline; links hemispheres electrically
  - Common average reference (CAR): unbiased in dense-coverage limit*

$$\Phi_i^{\mathrm{CAR}}(t) = \Phi_i(t) - \frac{1}{N}\sum_{j=1}^{N}\Phi_j(t)$$

- REST (Yao 2001) [31]: model-based analytical ref at infinity; accuracy bounded by head model
  - Surface Laplacian / CSD: reference-free; needs ≥ 10–10

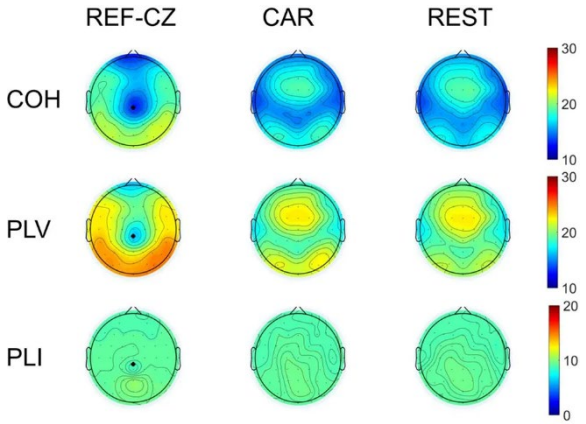

Zhang L et al., (2020)
Front. Hum. Neurosci. 14:367

Making Jansen–Rit Predict EEG: The W08 Observation Model

- W08 framing: $y_1 - y_2$ = population-averaged PSP (mV), NOT a current dipole moment. 'Simulated EEG' requires observation model.

- 5-step recipe:
  1. Gain: g maps $y_1 - y_2 \rightarrow$ dipole density $q(t) = g \cdot (y_1 - y_2)$
  2. Spatial integration: $Q(t) = q(t) \cdot A$ over the active cortical patch
  3. Cortical placement: Q(t) on cortical mesh w/ local surface normal
  4. Lead-field: dipole vector $\mathbf{p}(t) = Q(t)\hat{\mathbf{n}} \Rightarrow \mathbf{v}(t) = \mathbf{L}\,\mathbf{p}(t)$
  5. Choose reference (CAR, REST, single-ref — see prev slide)

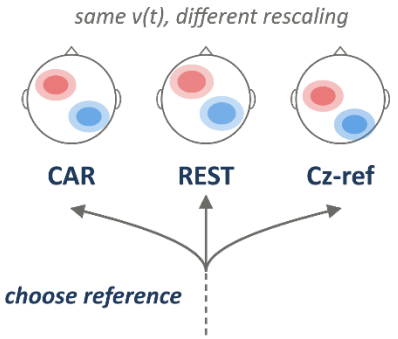

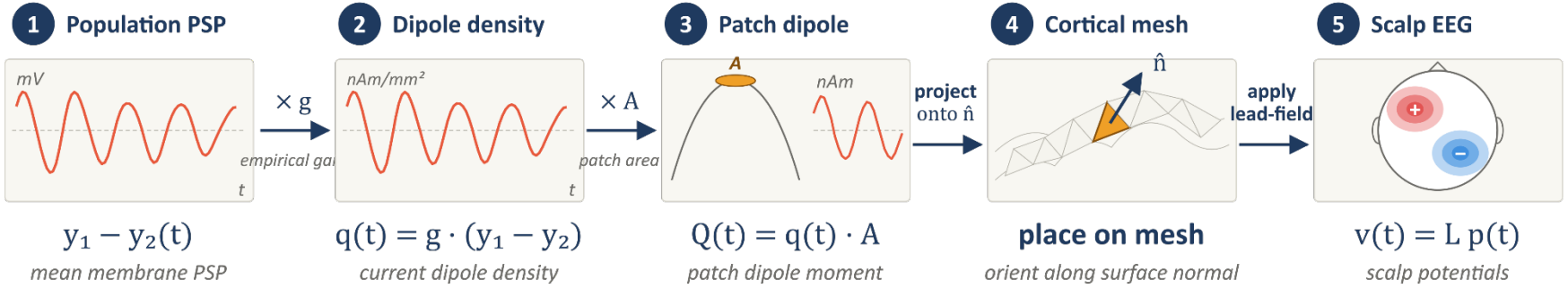

Outline for Today

- Extracellular Potentials at the Source — MUA, LFP, CSD
- Scalp-Level Signals — EEG, MEG, electrode layouts, reference problem
- **The EEG Forward Problem — Poisson BVP, lead-field matrix, tissue conductivities**
- The Reciprocity Theorem — Helmholtz 1853 → modern lead-field theory → tES
- Other Recording Modalities — fMRI/BOLD and eCAPs
- Engagement Metrics & Summary — Exposure vs. response, pivot to W10
- Exercise Preview — Mini project work

The EEG Forward Problem: A Poisson Boundary-Value Problem (BVP)

- Quasi-static justification (Plonsey & Heppner 1967, invoking W04) [33]: at bioelectric frequencies, displacement & inductive effects negligible:
  - $\nabla \times \mathbf{E} = 0 \rightarrow \mathbf{E} = -\nabla V$
  - $\nabla \cdot \mathbf{J_{total}} = 0,\ \mathbf{J_{total}} = \sigma \mathbf{E} + \mathbf{J^p}$
- Combining → core equation: $\boxed{\nabla \cdot [\sigma(\mathbf{r}) \nabla V(\mathbf{r})] = \nabla \cdot \mathbf{J^p}(\mathbf{r})}$
- Source term: impressed current density $\mathbf{J^p}(\mathbf{r})$ — arbitrary in general; scalar source form: $I_v = -\nabla \cdot \mathbf{J^p}(\mathbf{r})$. Common specialization for source analysis is the **point dipole** at $\mathbf{r_0}$,

$$\mathbf{J^p}(\mathbf{r}) = \mathbf{p}\, \delta^3(\mathbf{r} - \mathbf{r_0})$$

- Boundary conditions:
  - Scalp–air (no current to air): $\sigma \partial V / \partial n|_{\partial \Omega} = 0$
  - Internal tissue interfaces: V continuous; normal $(\sigma \nabla V) \cdot \mathbf{n}$ continuous
  - Reference potential fixed for uniqueness

Wang C. et al. *PLoS ONE* 9(11): e113264.

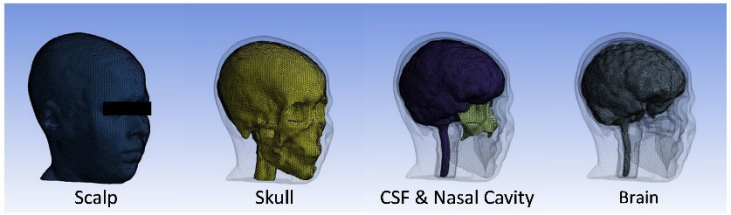

(a)

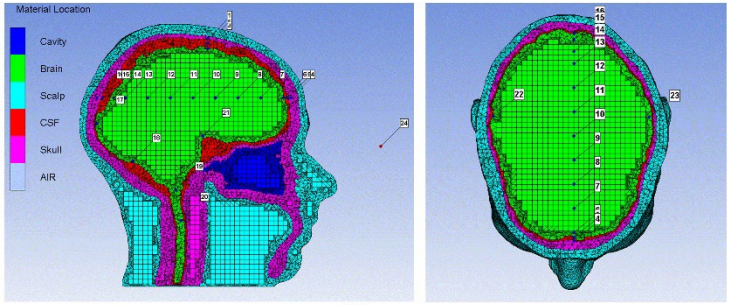

(b)

Lead-Field Matrix: Linearity Buys You Everything

- Poisson BVP linear in V + source → source→sensor map = linear operator, discretized as lead-field matrix L: $\boxed{\mathbf{V} = \mathbf{LJ} + \boldsymbol{\varepsilon}}$
- Dimensions:
  - Free-orientation dipoles (N_s sensors, N_d dipole locations):
    $$\mathbf{L} \in \mathbb{R}^{(N_s \times 3N_d)}$$
  - Fixed (cortically-normal) orientation:
    $$\mathbf{L} \in \mathbb{R}^{(N_s \times N_d)}$$
- Row interpretation (reciprocity-based):
  - Row $L_{i,:}$ = elec_i's spatial sensitivity inside head
  - Reciprocity theorem (Part IV) → = E-field inside the head from unit current (w.r.t. ref.) at elec_i

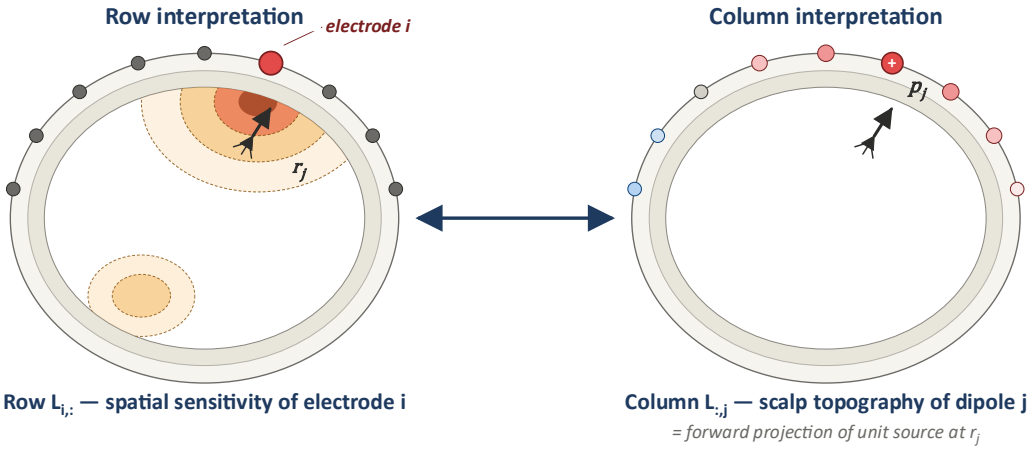

- Column interpretation:
  - Each column triplet (x,y,z per dipole location) = scalp topography of unit dipole at one source location
- **L** discretizes a more general reciprocity map — any volume-source distribution projects to sensors via the same underlying identity; the dipole basis is the standard discretization.
- Why it matters:
  - Once **L** computed, forward prediction = matrix-vector product
  - Inverse problem → (regularized) matrix inversion (Slide 25)
  - Source localization, connectivity analysis, dynamic causal models (DCM) — all rest on **L**

Computing the Lead-Field: BEM, FEM, FDM

- Methods (Hallez 2007 review) [32]:

Method	Geometry	Pros	Cons	Ref
n-sphere analytical	concentric spheres	closed form; benchmark	unrealistic	Zhang [34]
boundary element method (BEM)	nested surfaces	surface degrees of freedom (DOFs) only; mature	assumes isotropy	[23, 35]
finite element method (FEM)	volumetric mesh	anisotropy, cerebrospinal fluid (CSF), defects	mesh gen; dipole singularity	Wolters [24]
finite difference method (FDM)	voxel grid	anisotropy; simple	staircase boundaries	—

Φ = interior potential; Φ_∞ = free-space potential for the same sources; $\sigma_k^{\pm}$ = conductivities on interior / exterior sides of interface S_k; r, r' = field- and source-points

- Geselowitz surface-integral (BEM):

$$\sigma\Phi(\mathbf{r}) = \sigma\Phi_\infty(\mathbf{r}) - \frac{1}{4\pi}\sum_k (\sigma_k^- - \sigma_k^+) \oint_{S_k} \Phi(\mathbf{r}') \frac{(\mathbf{r}-\mathbf{r}')\cdot d\mathbf{S}'}{|\mathbf{r}-\mathbf{r}'|^3}$$

- Production pipelines: Sim4Life (FEM/FDM) · SimNIBS (FEM) · OpenMEEG (BEM) · FieldTrip+SimBio (FEM) · MNE-Python · ROAST
- Transfer-matrix trick (Mosher 1999; Wolters 2006): 1 forward solve per electrode → full L — anticipates Part IV reciprocity

The EEG Inverse Problem: Why It's Hard

- Underdetermined & ill-posed: $N_s \ll 3N_d \rightarrow \infty$ solutions match V; noise amplification, radial-dipole null space, deep-source attenuation (prior knowledge/constraints needed)
- Tikhonov-regularized minimum-norm [41]:

$$\hat{\mathbf{J}} = (\mathbf{L}^\top \mathbf{L} + \lambda \mathbf{I})^{-1} \mathbf{L}^\top \mathbf{V}$$

$\hat{J}$ = regularized source estimate, λ = regularization parameter, I = identity

- Method lineage:

Method	Feature
minimum-norm estimate (MNE)	ℓ_2 min-norm; free or fixed orientation [41]
low-resolution electromagnetic tomography (LORETA)	smoothness via Laplacian regularizer [42]
standardized LORETA (sLORETA)	standardized MNE; zero bias only under idealized assumptions [43]
LCMV beamformer	adaptive spatial filter; orthogonal to source covariance [44]

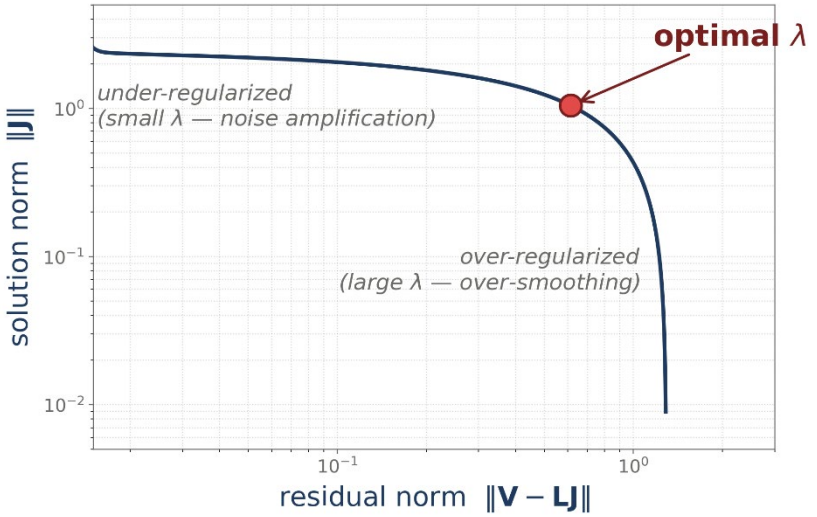

- LCMV closed form: $\mathbf{w}(\mathbf{r}) = \frac{\mathbf{R}^{-1}\mathbf{l}(\mathbf{r})}{\mathbf{l}(\mathbf{r})^\top \mathbf{R}^{-1}\mathbf{l}(\mathbf{r})}$
- Takeaway: no universally best method — method choice = source-model choice (sparse vs. distributed, focal vs. extended, single vs. multiple)

w(r) = spatial filter; l(r) = forward column at r (column of L); R = data covariance

Outline for Today

- Extracellular Potentials at the Source — MUA, LFP, CSD
- Scalp-Level Signals — EEG, MEG, electrode layouts, reference problem
- The EEG Forward Problem — Poisson BVP, lead-field matrix, tissue conductivities
- **The Reciprocity Theorem — Helmholtz 1853 → modern lead-field theory → tES**
- Other Recording Modalities — fMRI/BOLD and eCAPs
- Engagement Metrics & Summary — Exposure vs. response, pivot to W10
- Exercise Preview — Mini project work

From Helmholtz 1853 to Modern Lead-Field Theory

- **Hermann von Helmholtz** (1821–1894) — 3 yrs after measuring nerve conduction velocity in frog sciatic (~25–43 m/s, W01 callback) [49], extended Green's 1828 reciprocal theorem from electrostatics → stationary conduction currents in inhomogeneous bodies [47, 48]

von Helmholtz

- Paraphrased: "*potential at B from current element at A = potential at A from same element at B, in a linear isotropic conductor*"

- Modern lineage:
  - Plonsey 1963 — restates Helmholtz using vector-calculus; used in most modern EEG/electrocardiography (ECG)/MEG source-analysis code [50]
  - Rush & Driscoll 1969 — applied reciprocity to EEG lead fields on 3-concentric-sphere head [22]
  - Malmivuo & Plonsey 1995 (Bioelectromagnetism Ch. 11) — definitive textbook treatment [52]

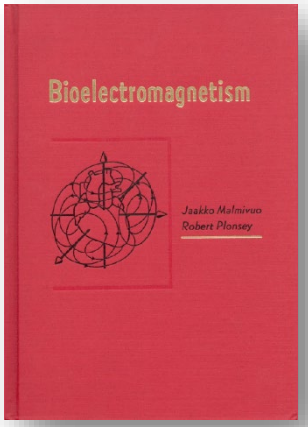

Quasi-static reduction (W04 callback):

$$\nabla \cdot [\sigma(\mathbf{r})\nabla\Phi(\mathbf{r})] = \nabla \cdot \mathbf{J}^{\mathbf{p}}(\mathbf{r})$$

Derivation: Reciprocity Theorem

- Setup: linear isotropic quasi-static conductor (Ω, σ(r)); two independent sources $\mathbf{J}^{\mathbf{p}}_{\mathbf{a,b}}$ with potentials $\Phi_{a,b}$.
- Step 1 — σ-weighted Green's second identity:

$$\int_{\Omega}[u\nabla\cdot(\sigma\nabla v)-v\nabla\cdot(\sigma\nabla u)]dV=\oint_{\partial\Omega}\sigma(u\partial_n v-v\partial_n u)dS$$

- Step 2 — Substitute $u=\Phi_a,\ v=\Phi_b$; use $\nabla\cdot(\sigma\nabla\Phi)=\nabla\cdot\mathbf{J}^{\mathbf{p}}$:

$$\int_{\Omega}\left[\Phi_a\nabla\cdot\mathbf{J}^{\mathbf{p}}_{\mathbf{b}}-\Phi_b\nabla\cdot\mathbf{J}^{\mathbf{p}}_{\mathbf{a}}\right]dV=\oint_{\partial\Omega}\sigma(\Phi_a\partial_n\Phi_b-\Phi_b\partial_n\Phi_a)dS$$

σ(r) = spatially-varying conductivity; Ω, ∂Ω = domain and boundary; $\mathrm{J}^{\mathrm{p}}_{\mathrm{a,b}}$ = two independent impressed-current densities with potentials $\Phi_{\mathrm{a,b}}$ and fields $E_{\mathrm{a,b}} = -\nabla\Phi_{\mathrm{a,b}}$; u, v = generic test functions in Green's identity; $\partial n \equiv n\cdot\nabla$ = outward normal derivative; I_b = injected current in configuration (b), entering at r+, leaving at r−

- Step 3 — Insulating scalp BC ($\sigma\partial_n\Phi=0$ except at electrodes) → surface integral → 0 for interior sources (so RHS vanishes).
- Step 4 — Transform LHS: integrate by parts ($\oint\Phi\ \mathbf{J}^p\cdot\hat{n}\,dS=0$ because $\mathbf{J}^{\mathbf{p}}$ vanishes on ∂Ω) → reciprocity identity ($\Phi\nabla\cdot\mathbf{J}^p=\nabla\cdot(\Phi\mathbf{J}^p)-\nabla\Phi\cdot\mathbf{J}^p$):

$$\int\Phi\nabla\cdot\mathbf{J}^p dV=\oint\Phi\mathbf{J}^p\cdot\hat{n}\,dS-\int\nabla\Phi\cdot\mathbf{J}^p dV=\int E\cdot\mathbf{J}^p dV\ \Rightarrow\ \text{(apply to both terms on LHS)}$$

$$\boxed{\int_{\Omega}\mathbf{J}^{\mathbf{p}}_{\mathbf{a}}\cdot\mathbf{E}_{\mathbf{b}}dV=\int_{\Omega}\mathbf{J}^{\mathbf{p}}_{\mathbf{b}}\cdot\mathbf{E}_{\mathbf{a}}dV}\qquad\text{(Helmholtz–Plonsey)}$$

- Step 5 — Electrode-pair form. I_b enters at r_+, leaves at r_-; boundary integral → surface terms over electrode patches:

$$I_b[\Phi_a(\mathbf{r}_+)-\Phi_a(\mathbf{r}_-)]=\int_{\Omega}\mathbf{J}^{\mathbf{p}}_{\mathbf{a}}\cdot\mathbf{E}_{\mathbf{b}}dV$$

- **General form** — Valid for any brain volume-source distribution; *no dipole assumption*; $I_v=-\nabla\cdot\mathbf{J}^{\mathbf{p}}$. Equivalent to Step 4 via integration by parts (with $\mathbf{E}=-\nabla\Phi$):

$$I_b V_{\mathrm{rec}}=-\int_V I_{v,a}(\mathbf{r})\Phi_{\mathrm{b}}(\mathbf{r})dV$$

Reciprocity

Key Result: $V_{\mathrm{rec}} = p \cdot E_{\mathrm{rec}}(r_0)/I$

- Point-dipole specialization of the general identity (prev. slide): set $\mathbf{J}_a^p = \mathbf{p}\,\delta^3(\mathbf{r}-\mathbf{r}_0) \Leftrightarrow I_{v,a} = -\mathbf{p}\cdot\nabla\delta^3(\mathbf{r}-\mathbf{r}_0)$.
- Source (a) = point dipole $\mathbf{p}$ at $\mathbf{r_0}$ (see above).
- Source (b) = reciprocal experiment: current I injected through same electrode pair produces field $\boldsymbol{E}_{\mathbf{rec}}$ throughout brain
- Substitute into Step 5:

$$IV_{\mathrm{rec}} = \int_{\Omega} [\mathbf{p}\delta^3(\mathbf{r}-\mathbf{r_0})]\cdot\mathbf{E_{rec}}(\mathbf{r})dV = \mathbf{p}\cdot\mathbf{E_{rec}}(\mathbf{r_0})$$

$$\boxed{V_{\mathrm{rec}} = \frac{\mathbf{p}\cdot\mathbf{E_{rec}}(\mathbf{r_0})}{I}}$$

- Lead-field vector:

$$\mathbf{L}(\mathbf{r_0}) \equiv \mathbf{E_{rec}}(\mathbf{r_0})/I \Rightarrow$$
$$V_{\mathrm{rec}} = \mathbf{p}\cdot\mathbf{L}(\mathbf{r_0})$$

- Lead-field = geometric property of conductor — independent of neural activity
- Computational shortcut (Rush & Driscoll 1969 insight) [22]: 1 forward transcranial electrical stimulation (tES) solve (unit current injection between the pair) → lead-field at every interior point simultaneously — basis of modern forward solvers

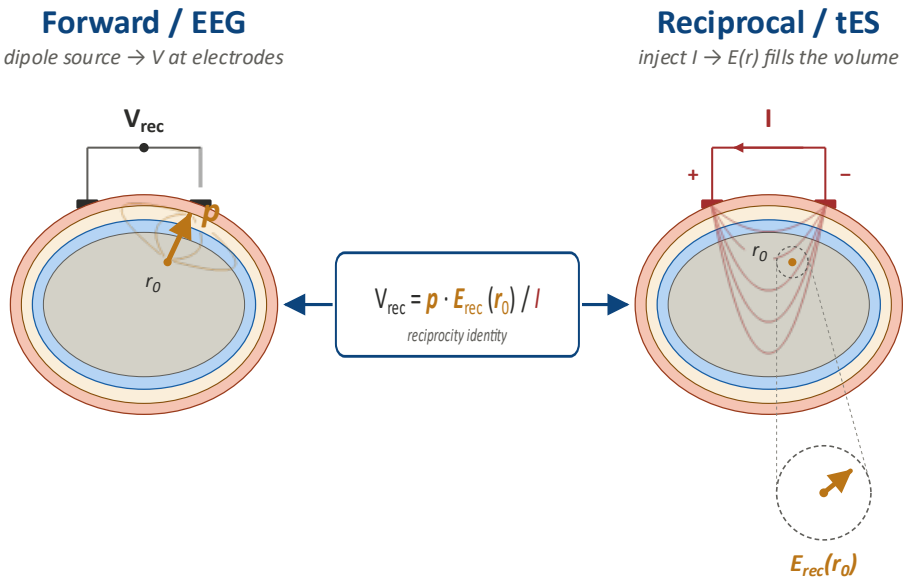

EEG and tES Are Duals of One Electromagnetic Problem

- Continuum: reciprocity → exact duality between EEG and tES forward operators
- Discretized (point dipole **p**; applied electrode-current vector **i**):

$$\mathbf{v} = \mathbf{L}\mathbf{p} \qquad \text{(forward EEG)}$$

$$\mathbf{E}_{\mathbf{brain}} = \mathbf{L}^{\mathrm{T}}\mathbf{i} \qquad \text{(forward tES)}$$

- Why transpose? L_{sj} couples electrode *s* to brain voxel *j*. The volume-conductor operator $\nabla\cdot(\sigma\nabla\cdot)$ is self-adjoint (σ symmetric), so this coupling is direction-independent. EEG sums over voxels (columns); tES sums over electrodes (rows).
- Take-home:
  - EEG source localization + tES current design = duals of same volume-conductor problem
  - 1 set of tES forward solves over all scalp electrodes → all columns of **L** efficiently
  - Reciprocity turns N_d-many dipole forward solves into N_s-many electrode forward solves — massive computational savings
- Consequence: same personalized head model serves measurement (EEG inverse) + intervention (tES design)

***N.B.** The time-dependence of current sources are separable from the spatial lead-field calculation; time-dependent EEG/tES signals can be trivially computed using temporally scaled source terms.

Optimal tES Montage = EEG Pattern the Target Would Produce

- **Goal** (Dmochowski 2011 [54]): pick currents **i** that drive the strongest E-field along **d** at target $\boldsymbol{r}_t$
- Reciprocity result: optimal montage = scalp voltage that target dipole would produce:

$$\mathbf{i}^\star \propto \mathbf{v}^\star$$

(Fernández-Corazza 2016 [53]). *One* EEG forward solve — not an optimization.
- *Diffuse by design:* maximizes intensity **at** the target, **not focality** elsewhere → focality is a different objective (W11)
- **Takeaway:** *naive tES montage = EEG pattern.* Exact, closed form.

target location r_t; target direction d (unit vector along which E is maximized); optimal electrode-current pattern $i^\star$ and corresponding optimal scalp-voltage pattern $v^\star$

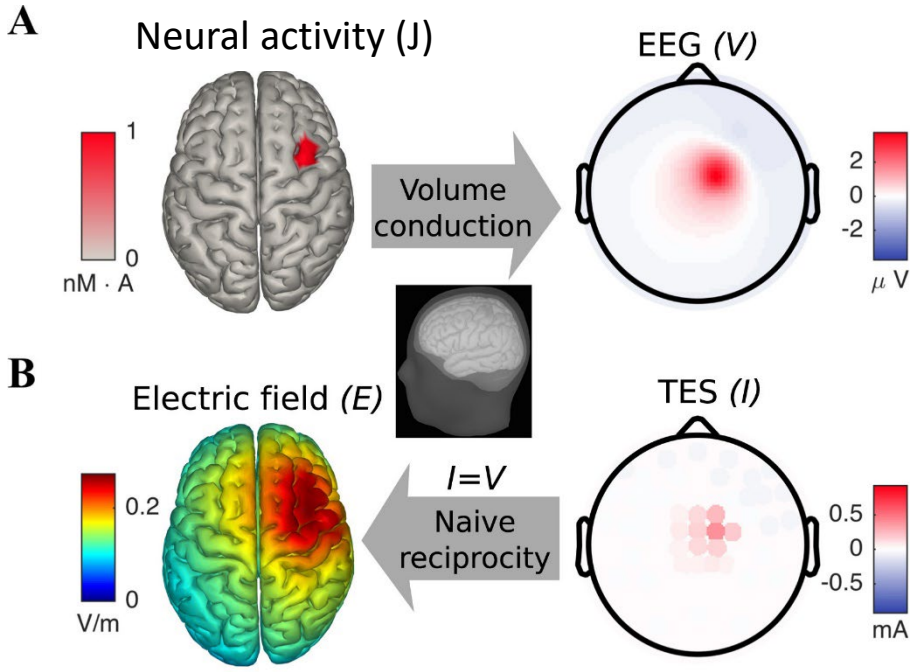

J. P. Dmochowski et al., *J. Neural Eng.*, vol. 8, no. 4, art. 046011, 2011

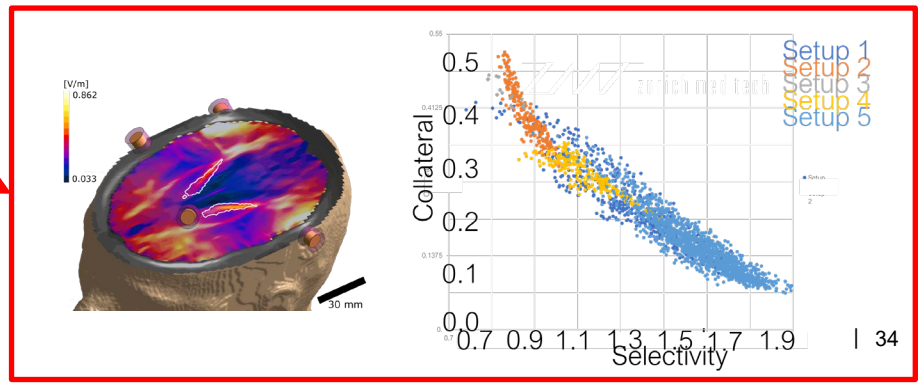

Outline for Today

- Extracellular Potentials at the Source — MUA, LFP, CSD
- Scalp-Level Signals — EEG, MEG, electrode layouts, reference problem
- The EEG Forward Problem — Poisson BVP, lead-field matrix, tissue conductivities
- The Reciprocity Theorem — Helmholtz 1853 → modern lead-field theory → tES
- **Other Recording Modalities — fMRI/BOLD and eCAPs**
- Engagement Metrics & Summary — Exposure vs. response, pivot to W10
- Exercise Preview — Mini project work

fMRI/BOLD: An Indirect, Hemodynamic Proxy

- **Neurovascular coupling** — *see cascade (right)*
- **Blood-oxygen-level-dependent (BOLD)** contrast: Ogawa 1990 (rodent 7–8.4 T); human task-based 1992 (Ogawa / Kwong / Bandettini) [57, 58]
- **Canonical hemodynamic response function (HRF)**: initial dip ~1 s (debated) · peak ~4–6 s · undershoot 10–20 s
- **Resolution**: 1–3 mm spatial (sub-mm at ≥ 7 T) · ~1–3 s temporal
- **vs. EEG/MEG** — complementary: direct neurophysiology @ ms ↔ hemodynamic proxy @ mm

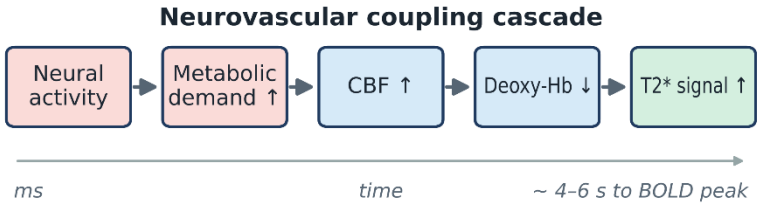

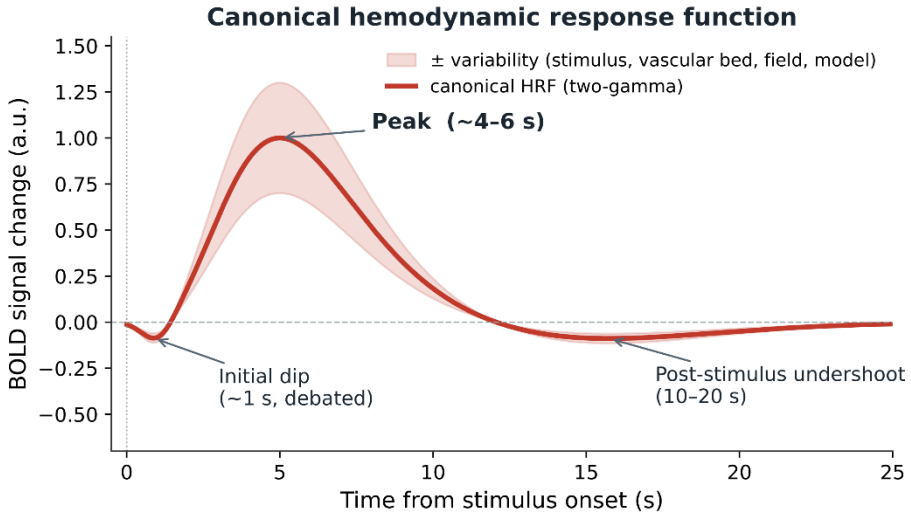

Balloon–Windkessel: A Biomechanical State-Space Model of BOLD

- Buxton, Wong & Frank 1998 — 2 state variables driven by cerebral blood flow (CBF) *f*(t) [59]:
  - v(t): normalized venous volume (*the "balloon"* — expands when inflow > outflow)
  - q(t): normalized deoxy-haemoglobin (deoxy-Hb) content

$$\tau \dot{v} = f - v^{1/\alpha}$$

$$\tau \dot{q} = f \frac{E(f, E_0)}{E_0} - v^{1/\alpha} \frac{q}{v}$$

α: Grubb exponent; τ: transit time; E_0: resting O_2 extraction; E(f, E_0): oxygen-extraction fraction, with resting value E_0

- BOLD signal:

$$\frac{\Delta S}{S_0} = V_0[k_1(1-q) + k_2(1-q/v) + k_3(1-v)]$$

- Interpretive limits (Logothetis 2008, canonical review) [62]:
  - BOLD reflects neural mass activity via complex, state-dependent coupling
  - Spatial resolution limited by draining-vein macrovasculature
  - CBF/ cerebral metabolic rate of O_2 ($CMRO_2$) coupling varies w/ inhibition + neuromodulation

V_0 = resting blood-volume fraction; k_1, k_2, k_3 = field-strength– and echo time (TE)-dependent coefficients; $\Delta S/S_0$ = fractional BOLD signal change relative to baseline S_0.

Pivotal finding (Logothetis et al. 2001) [61]: Macaque primary visual cortex (V1): LFP predicts BOLD better than MUA → synaptic/dendritic input, not spike output, is dominant driver

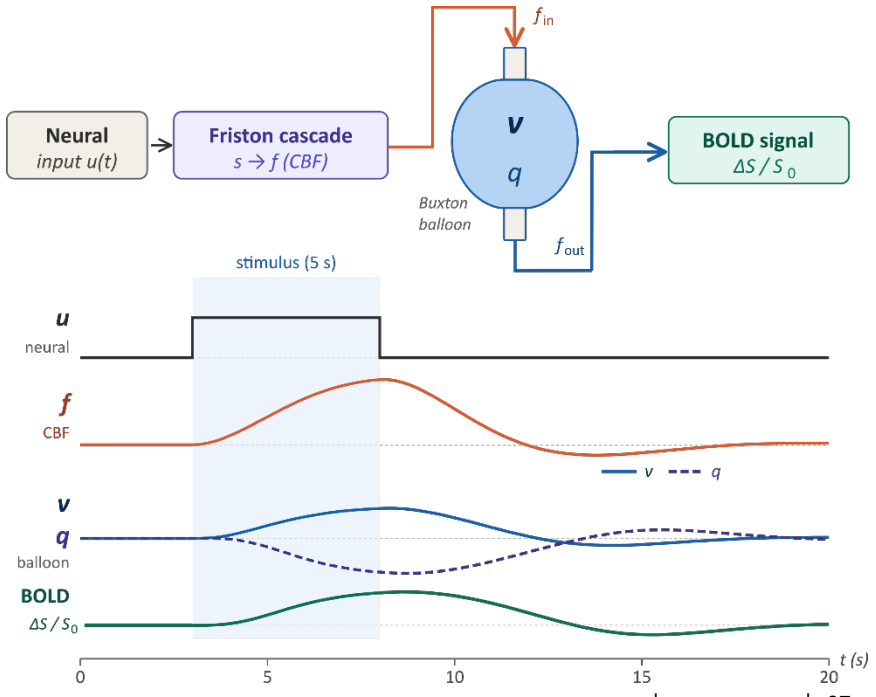

What is an eCAP?

- evoked compound action potential (**eCAP**) = near-field extracellular sum of synchronous single-fibre APs in stimulated bundle (dorsal column, vagus, auditory nerve)
- Parker et al. 2012 [63] — first minimally-invasive human spinal-cord eCAP during SCS:
  - Triphasic waveform, sub-ms to few-ms latencies
  - Aβ (large-diameter) fibers recruited at therapeutic amplitudes; clear threshold below which no eCAP measurable
- Waveform → biophysics:
  - Latency → conduction velocity → fiber diameter (Hursh 1939: $v \approx 6 \cdot d$ for myelinated axons — W05 callback)
  - Amplitude ∝ synchronously recruited fibres in first recruited population (**but not quite! → next slides**)
  - Orthodromic vs. antidromic separable by electrode position
- Clinical motivation: closed-loop bioelectronic medicine needs biomarkers from the nerve itself — e.g. NeuHeart [76]: intrafascicular cardiac-branch vagus nerve stimulation (VNS) to restore autonomic cardiac control after heart transplantation

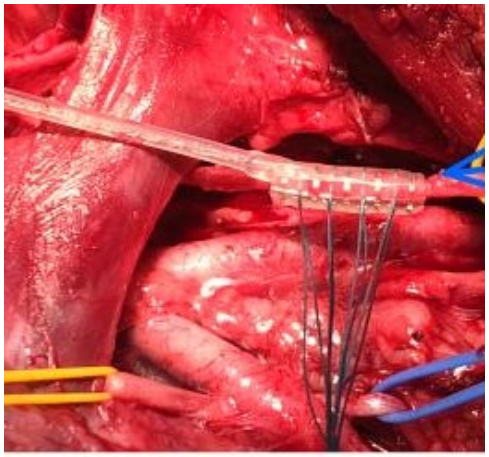

In-vivo cuff recording on porcine vagus nerve [76].

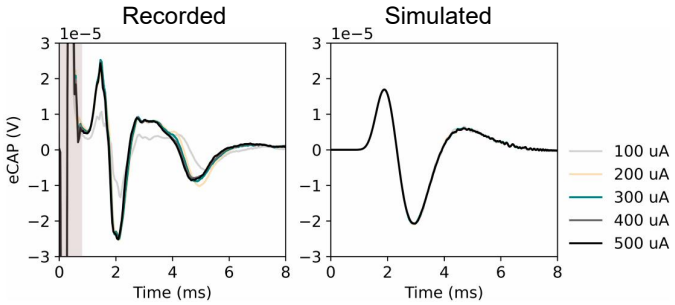

Representative porcine VNS eCAPs at increasing stimulus currents [76].

Modeling the Multifascicular eCAP

- Challenge: pig vagus nerve has >300,000 fibers across ~40 fascicles, mixed myelinated/unmyelinated — direct FEM per fiber is infeasible [76]
- Extended reciprocity theorem [76] generalizes the point-dipole identity from Slide 29 to a 1-D spatially extended current source along a fiber:

$$S(t) = \int_0^1 \Phi(l')i(l',t)dl'$$

- **Φ(l′)** is the fascicle sensitivity function, computed once per recording montage
- Semi-analytic pipeline [76]:
  - FEM of stimulation + recording electrodes → sensitivity function $\Phi_i(l)$ per fascicle
  - Coupled EM-electrophysiology → recruitment curves $R_i(d, I)$
  - Representative AP waveform $V_t(t)$ from NEURON fiber models [38]
  - Sum over fiber types × diameters × fascicles
- Speedup: ~5000× vs. per-fiber NEURON simulation, while retaining heterogeneous dielectric environments [76]
- Validated against porcine VNS with intrafascicular stimulation & 4-contact cuff recording

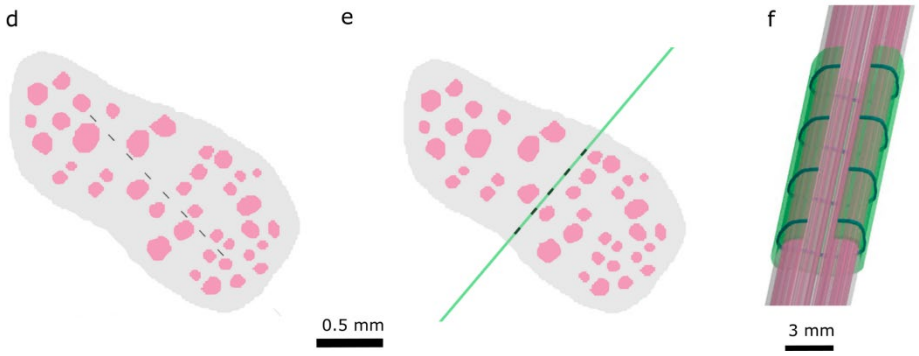

Model geometry: histology-based nerve cross-section + stimulation electrode in horizontal/vertical orientations, cuff recording (adapted from [76] Fig. 1).

Surprise!: eCAP Amplitude is Non-Monotonic in Recruitment

Dispersion in activated-fiber diameters cancels the signal

- Two cancellations stack [76]:
  - Single fiber: current conservation (Slide 10) gives zeroth-order cancellation; ± lobes of $\partial^2 V/\partial l^2$ and $\partial^2 \Phi/\partial l^2$ largely annihilate
  - Fiber population: smoothly varying diameters → shifted single-fiber action potential (SFAP) arrival times → additional cancellation
- *Consequence*: fully-activated fascicles quieter than expected; only partially-activated fascicles contribute strongly — sharp cutoff in recruited diameters → residual signal
- Peak eCAP amplitude is non-monotonic in stimulus current, and in activation fraction
- Fascicles cluster into recruitment-similar groups that dominate different time windows of the eCAP

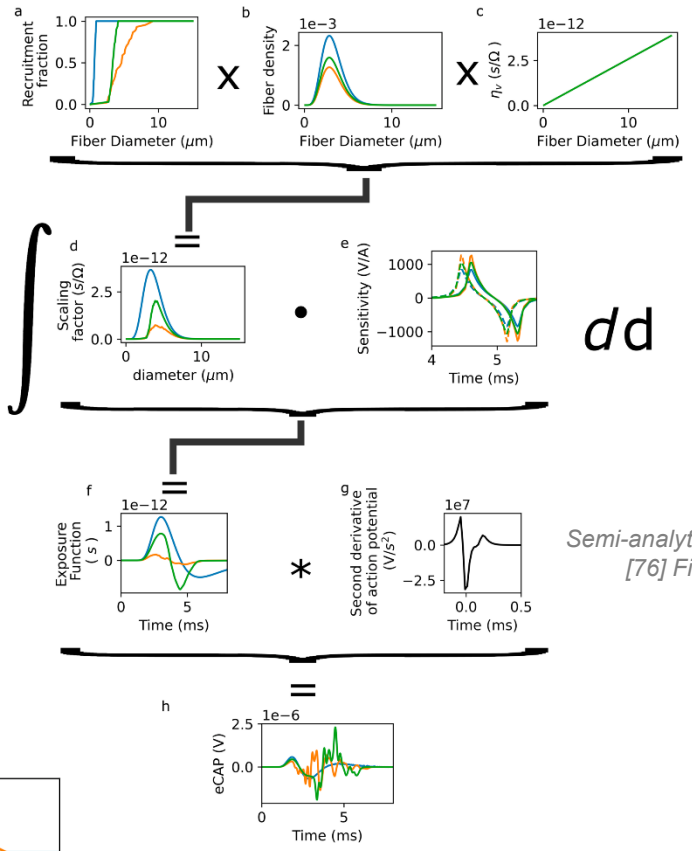

Semi-analytic pipeline [76] Fig. 5.

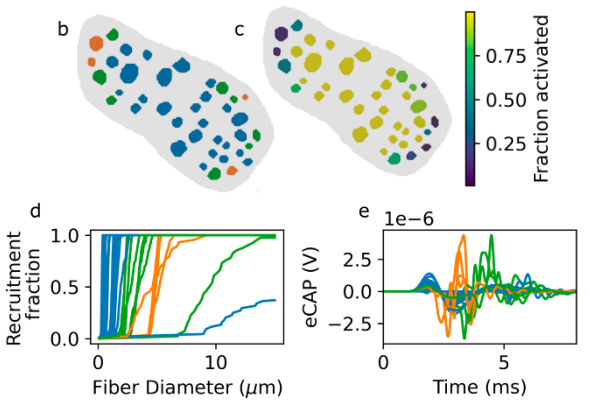

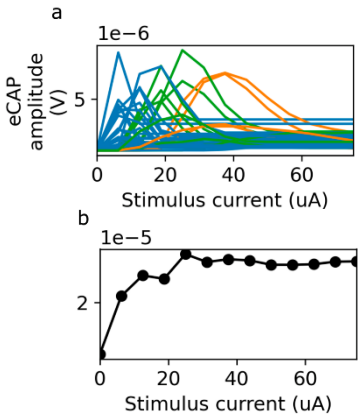

Left: Fascicle activation & k-means clustering into 3 groups (b, c) [76] Fig. 7.

Right: Per-fascicle (a) and total (b) peak eCAP vs. stimulus current [76] Fig. 8.

eCAP Shape Depends on Electrode Geometry

Stimulation and recording configuration shape the signal's information content

- Stimulus electrode orientation → which fascicles activate first → different eCAP waveform [76]
  - Insertion angle is a design variable, not a given
- Recording electrode span + circumferential position → which fascicles are visible in the sensitivity function $\Phi_i(I)$ [76]
- Bipolar vs. monopolar montage [76]:
  - Bipolar ≈ finite-difference derivative of monopolar → adds one signal lobe, emphasizes higher-frequency content
  - Contact separation controls derivative coarseness: small = true derivative; large → two separated monopolar recordings
- Consequence: model lets you design for information content — pick geometry that maximizes sensitivity to the feature you want to decode (fiber-type selectivity, fascicle identity, …)

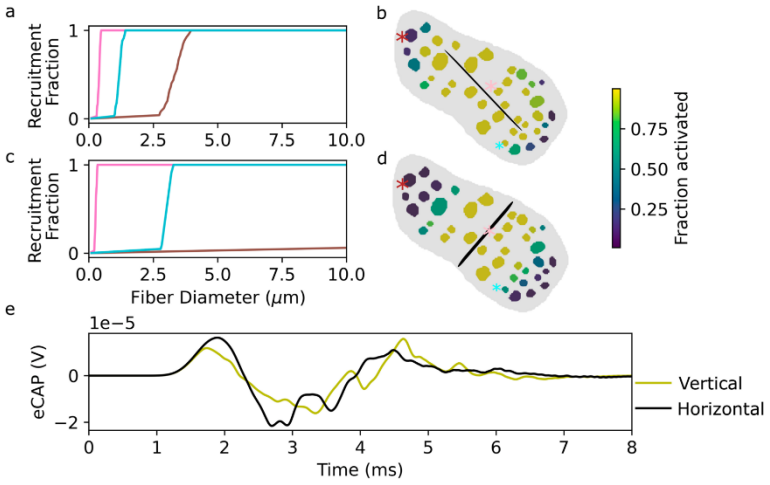

Stim. orientation: different fascicular activation, different eCAP [76] Fig. 9.

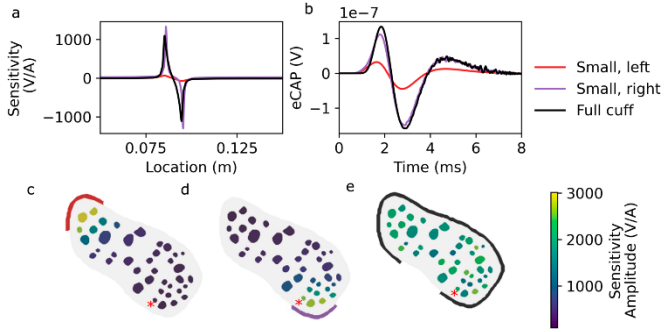

Stimulus electrode orientation influences eCAP due to differential activation of fascicles

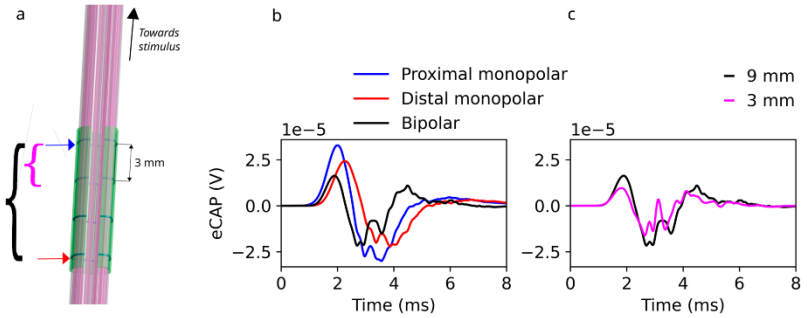

Monopolar vs. bipolar recording; 3 mm vs. 9 mm contact separation [76] Fig. 11.

Inverse Problem: Fitting Model Parameters

Model + measurement → recover fiber population statistics

- Inverse problem: fit model parameters (e.g., fiber-diameter distribution shape + scale) to minimize $\|V_{\text{model}} - V_{\text{measured}}\|_1$
- Proof-of-concept [76]: starting from arbitrary parameters, optimization recovers ground-truth fiber-diameter distribution in ~200 iterations (relative error $<10^{-3}$ on shape & scale)
- In vivo caveats: degeneracy (multiple parameter combos can match one signal), tissue-property uncertainty, inter-subject anatomical variability
  - Mitigable by multiple stimulus/electrode configurations and complementary imaging
- **Clinical reality**: *complexity doesn't preclude utility* — eCAP-controlled closed-loop SCS (Evoke RCT [64]) outperforms open-loop despite using eCAP amplitude as a blunt biomarker. Model-based interpretation moves the field from blunt to sharp.
- Pivot to W10: next week we solve the forward problem for stimulation (transcranial direct-current (tDCS), alternating-current (tACS), magnetic (TMS), and temporal interference (TI) stimulation); the same multiscale reciprocity-based framework applies

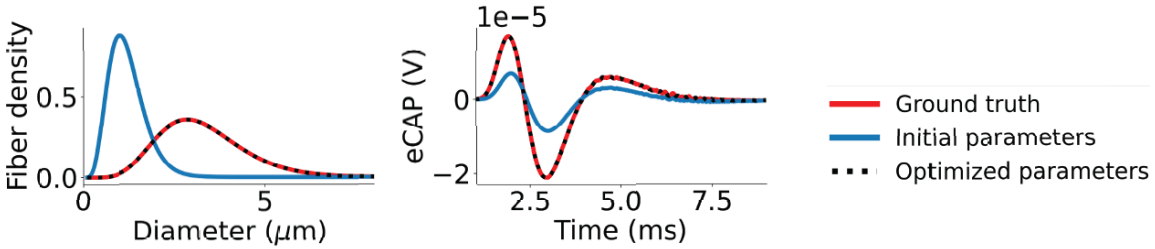

Fiber-diameter distribution recovered from eCAP by parameter optimization [76] Fig. 12.

Outline for Today

- Extracellular Potentials at the Source — MUA, LFP, CSD
- Scalp-Level Signals — EEG, MEG, electrode layouts, reference problem
- The EEG Forward Problem — Poisson BVP, lead-field matrix, tissue conductivities
- The Reciprocity Theorem — Helmholtz 1853 → modern lead-field theory → tES
- Other Recording Modalities — fMRI/BOLD and eCAPs
- **Engagement Metrics & Summary — Exposure vs. response, pivot to W10**
- Exercise Preview — Mini project work

From Exposure to Response

- Old paradigm — exposure-based metrics ("dose"):
  - |E|, specific absorption rate (SAR) (RF/ultrasound analogs), volume of tissue activated (VTA)
  - Butson et al. 2007 [68], patient-specific VTA: FEM + cable-model axon thresholds + activating functions — dominant deep brain stimulation (DBS) dose surrogate
  - Critique: exposure metrics describe what field does to tissue, not neural response
  - Open-loop, blind to state/plasticity/engagement; patients w/ identical VTAs can diverge clinically
- New paradigm — response-based metrics:

Modality	Response metric	Scale
EEG/MEG	Spectral power shift, event-related potential (ERP), TMS-evoked potential (TEP)	macro (cm)
fMRI	BOLD %-signal change	macro (cm)
ECoG/intracranial EEG (iEEG)	High-γ (70–150 Hz) power, phase-locking	meso (mm)
Peripheral/spinal	eCAP amplitude	meso (µm–mm)
Multielectrode array (MEA)	Spike rate, evoked potential	micro (µm)

- Key feature — closed-loop compatible: response metrics fed back in real time
- Shift: forward-only "delivered dose" → closed-loop "measured engagement"

Criteria for Engagement Metrics

- Necessary criteria, synthesized from Polanía, Nitsche & Ruff 2018 [69] + Bergmann & Hartwigsen 2021 [70]:
  - Computable from mechanistic model → forward simulation yields specific prediction, not curve fit
  - Measurable in vivo → existing instrumentation at relevant scale
  - Biophysically interpretable → each link in causal chain identifiable
  - Specific, sensitive, robust → resilient to confounders (arousal, drift, peripheral sensation)
  - Falsifiable → model→metric chain allows metric to be wrong
- Any quantity not clearing these criteria = correlate, not mechanism — closed-loop medicine requires causal mechanisms, not correlation
- 5-step causal chain (Bergmann & Hartwigsen): stimulus → E-field → local activity → network → cognition → behavior/physiology (e.g., blood pressure)

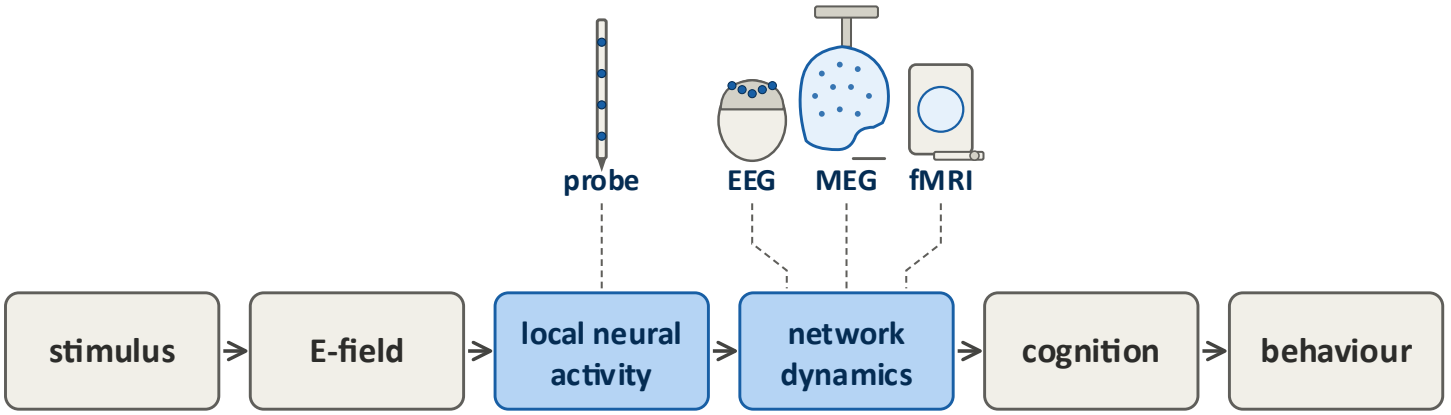

Adapted from Bergmann & Hartwigsen 2021 [70]

Recording Modality Determines Output Space

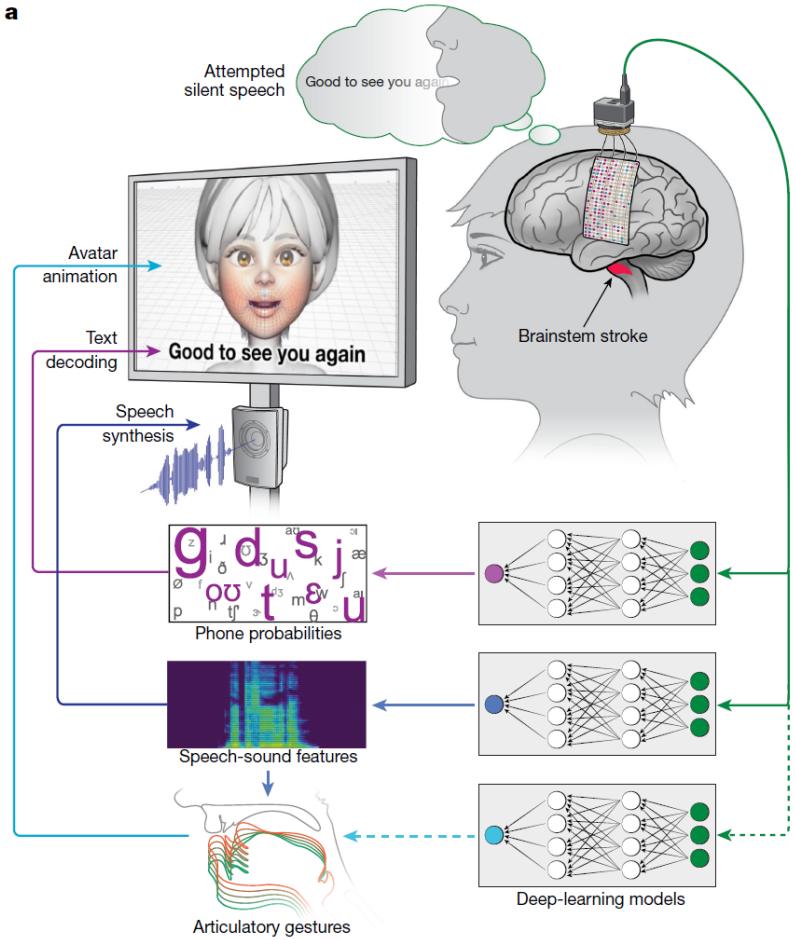

Metzger *et al. Nature* **620**, 1037–1046 (2023)

- Metzger et al. — "A high-performance neuroprosthesis for speech decoding and avatar control" [72]
- ECoG high-γ (70–150 Hz) decoded in parallel to three outputs in one patient:
  - Text — word-level natural-language decoding
  - Synthesized speech — audio waveform
  - Animated avatar — facial expressions
- Why this case study:
  - 3 recording→output chains in one paper make the point: "recording modality determines output space"
  - ECoG at mesoscale between BrainGate intracortical [73] + scalp EEG — completes spatial-scale arc
  - High-γ power = biophysically interpretable, model-predictable response metric from slides 39/40

Key Takeaways; Bridge to Next Week

1. Recording modalities span >6 orders of magnitude in spatial scale — from whole-cell patch clamp (single-neuron compartment) to whole-head EEG/MEG (macro)
2. Every measurement is a forward model:
   - $V_e \propto \sigma^{-1} \times \sum i_{mem}$ (Part I)
   - EEG = L · J (Parts II–III)
   - BOLD = hemodynamic kernel * LFP-like drive (Part V)
   - eCAP = line-source sum on a cylindrical nerve (Part V)
3. Reciprocity unifies recording and stimulation — the same lead-field matrix maps dipoles → electrodes (EEG, Part III) and electrode currents → brain E-field (tES, W10). Measurement and intervention are duals of one electromagnetic problem (Part IV)
4. Response → exposure for closed-loop control — exposure metrics (|E|, SAR, VTA) are open-loop; response metrics (EEG, BOLD, eCAP, spike rate) close the loop
5. Pivot to W10 — flip the arrow: next week we solve the forward problem for stimulation (tES/tDCS/tACS/TMS/TI), with diffusion-weighted/tensor imaging (DWI/DTI)-informed tissue conductivities in W11, so we can simulate both dose and response metrics on the same head model

MEG Scanner

Image: NIMH Image library, http://infocenter.nimh.nih.gov/il/public_il/image_details.cfm?id=80, Public Domain, https://commons.wikimedia.org/w/index.php?curid=11909237

Exercise: Mini Project Work Session

- **This week:** dedicated time for supervised mini project work
- Apply concepts from Weeks 1–8 to your chosen project topic
- Consider the abstraction-level question for your own project:
  - What is the minimum level of biophysical detail your question requires?
  - Where can you simplify without changing the answer?
- Office hours available for project consultation
- **Reminder:** project presentations in Week 13 (28.05.2026)

Upcoming guest lecture schedule:

- **April 30th**: Prof. Reto Huber (Zurich Children's Hospital)—*Electric and Acoustic Brain Stimulation*
- **May 7th**: Prof. Henri Lorach (UNIL)—*Spinal Cord Stimulation*

References

[1] G. R. Holt and C. Koch, "Electrical interactions via the extracellular potential near cell bodies," J. Comput. Neurosci., vol. 6, no. 2, pp. 169–184, 1999.
[2] G. Buzsáki, C. A. Anastassiou, and C. Koch, "The origin of extracellular fields and currents — EEG, ECoG, LFP and spikes," Nat. Rev. Neurosci., vol. 13, no. 6, pp. 407–420, 2012.
[3] G. Buzsáki, "Large-scale recording of neuronal ensembles," Nat. Neurosci., vol. 7, no. 5, pp. 446–451, 2004.
[4] D. A. Henze et al., "Intracellular features predicted by extracellular recordings in the hippocampus in vivo," J. Neurophysiol., vol. 84, no. 1, pp. 390–400, 2000.
[5] R. Quian Quiroga, Z. Nadasdy, and Y. Ben-Shaul, "Unsupervised spike detection and sorting with wavelets and superparamagnetic clustering," Neural Comput., vol. 16, no. 8, pp. 1661–1687, 2004.
[6] G. T. Einevoll et al., "Modelling and analysis of local field potentials for studying the function of cortical circuits," Nat. Rev. Neurosci., vol. 14, no. 11, pp. 770–785, 2013.
[7] S. Łęski et al., "Frequency dependence of signal power and spatial reach of the local field potential," PLoS Comput. Biol., vol. 9, no. 7, e1003137, 2013.
[8] R. Lorente de Nó, "Analysis of the distribution of the action currents of nerve in volume conductors," Stud. Rockefeller Inst. Med. Res. Repr., vol. 132, pp. 384–477, 1947.
[9] C. Nicholson and J. A. Freeman, "Theory of current source-density analysis and determination of conductivity tensor for anuran cerebellum," J. Neurophysiol., vol. 38, no. 2, pp. 356–368, 1975.
[10] U. Mitzdorf, "Current source-density method and application in cat cerebral cortex," Physiol. Rev., vol. 65, no. 1, pp. 37–100, 1985.
[11] K. H. Pettersen et al., "Current-source density estimation based on inversion of electrostatic forward solution," J. Neurosci. Methods, vol. 154, pp. 116–133, 2006.
[12] S. Łęski et al., "Inverse current source density method in two dimensions," Neuroinformatics, vol. 9, no. 4, pp. 401–425, 2011.
[13] J. Potworowski et al., "Kernel current source density method," Neural Comput., vol. 24, no. 2, pp. 541–575, 2012.
[14] E. Hagen et al., "Hybrid scheme for modeling local field potentials from point-neuron networks," Cereb. Cortex, vol. 26, no. 12, pp. 4461–4496, 2016.
[15] C. Rössert et al., "Automated point-neuron simplification of data-driven microcircuit models," arXiv:1604.00087, 2016/17.
[16] H. Berger, "Über das Elektrenkephalogramm des Menschen," Arch. Psychiat. Nervenkrankh., vol. 87, pp. 527–570, 1929.
[17] P. L. Nunez and R. Srinivasan, Electric Fields of the Brain: The Neurophysics of EEG, 2nd ed. Oxford Univ. Press, 2006.
[18] S. Murakami and Y. Okada, "Contributions of principal neocortical neurons to MEG and EEG signals," J. Physiol., vol. 575, no. 3, pp. 925–936, 2006.
[19] S. Murakami and Y. Okada, "Invariance in current dipole moment density across brain structures and species," NeuroImage, vol. 111, pp. 49–58, 2015.
[20] J. Sarvas, "Basic mathematical and electromagnetic concepts of the biomagnetic inverse problem," Phys. Med. Biol., vol. 32, no. 1, pp. 11–22, 1987.
[21] M. Hämäläinen, R. Hari, R. J. Ilmoniemi, J. Knuutila, and O. V. Lounasmaa, "Magnetoencephalography — theory, instrumentation, and applications to noninvasive studies of the working human brain," Rev. Mod. Phys., vol. 65, no. 2, pp. 413–497, 1993.
[22] S. Rush and D. A. Driscoll, "EEG electrode sensitivity — an application of reciprocity," IEEE Trans. Biomed. Eng., vol. BME-16, no. 1, pp. 15–22, 1969.
[23] M. S. Hämäläinen and J. Sarvas, "Realistic conductivity geometry model of the human head for interpretation of neuromagnetic data," IEEE Trans. Biomed. Eng., vol. 36, no. 2, pp. 165–171, 1989.
[24] C. H. Wolters et al., "Influence of tissue conductivity anisotropy on EEG/MEG field and return current computation in a realistic head model," NeuroImage, vol. 30, no. 3, pp. 813–826, 2006.
[25] D. Cohen, "Magnetoencephalography: evidence of magnetic fields produced by alpha-rhythm currents," Science, vol. 161, pp. 784–786, 1968.
[26] D. Cohen, "Magnetoencephalography: detection of the brain's electrical activity with a superconducting magnetometer," Science, vol. 175, pp. 664–666, 1972.
[27] S. Baillet, "Magnetoencephalography for brain electrophysiology and imaging," Nat. Neurosci., vol. 20, no. 3, pp. 327–339, 2017.
[28] H. H. Jasper, "The ten-twenty electrode system of the International Federation," Electroencephalogr. Clin. Neurophysiol., vol. 10, pp. 371–375, 1958.
[29] G. H. Klem, H. O. Lüders, H. H. Jasper, and C. Elger, "The ten-twenty electrode system of the International Federation," EEG Clin. Neurophysiol. Suppl., vol. 52, pp. 3–6, 1999.
[30] R. Oostenveld and P. Praamstra, "The five percent electrode system for high-resolution EEG and ERP measurements," Clin. Neurophysiol., vol. 112, no. 4, pp. 713–719, 2001.

References

[31] D. Yao, "A method to standardize a reference of scalp EEG recordings to a point at infinity," Physiol. Meas., vol. 22, pp. 693–711, 2001.
[32] H. Hallez et al., "Review on solving the forward problem in EEG source analysis," J. NeuroEng. Rehabil., vol. 4, art. 46, 2007.
[33] R. Plonsey and D. B. Heppner, "Considerations of quasi-stationarity in electrophysiological systems," Bull. Math. Biophys., vol. 29, no. 4, pp. 657–664, 1967.
[34] Z. Zhang, "A fast method to compute surface potentials generated by dipoles within multilayer anisotropic spheres," Phys. Med. Biol., vol. 40, pp. 335–349, 1995.
[35] J. C. Mosher, R. M. Leahy, and P. S. Lewis, "EEG and MEG: forward solutions for inverse methods," IEEE Trans. Biomed. Eng., vol. 46, no. 3, pp. 245–259, 1999.
[36] S. B. Baumann et al., "The electrical conductivity of human cerebrospinal fluid at body temperature," IEEE Trans. Biomed. Eng., vol. 44, no. 3, pp. 220–223, 1997.
[37] K. Wendel et al., "The influence of CSF on EEG sensitivity distributions of multilayered head models," IEEE Trans. Biomed. Eng., vol. 55, no. 4, pp. 1454–1456, 2008.
[38] T. F. Oostendorp, J. Delbeke, and D. F. Stegeman, "The conductivity of the human skull: results of in vivo and in vitro measurements," IEEE Trans. Biomed. Eng., vol. 47, no. 11, pp. 1487–1492, 2000.
[39] M. Dannhauer, B. Lanfer, C. H. Wolters, and T. R. Knösche, "Modeling of the human skull in EEG source analysis," Hum. Brain Mapp., vol. 32, no. 9, pp. 1383–1399, 2011.
[40] M. Akhtari et al., "Conductivities of three-layer live human skull," Brain Topogr., vol. 14, pp. 151–167, 2002.
[41] M. S. Hämäläinen and R. J. Ilmoniemi, "Interpreting magnetic fields of the brain: minimum norm estimates," Med. Biol. Eng. Comput., vol. 32, no. 1, pp. 35–42, 1994.
[42] R. D. Pascual-Marqui, C. M. Michel, and D. Lehmann, "Low resolution electromagnetic tomography," Int. J. Psychophysiol., vol. 18, no. 1, pp. 49–65, 1994.
[43] R. D. Pascual-Marqui, "Standardized low-resolution brain electromagnetic tomography (sLORETA)," Methods Find. Exp. Clin. Pharmacol., vol. 24, Suppl. D, pp. 5–12, 2002.
[44] B. D. Van Veen, W. van Drongelen, M. Yuchtman, and A. Suzuki, "Localization of brain electrical activity via linearly constrained minimum variance spatial filtering," IEEE Trans. Biomed. Eng., vol. 44, no. 9, pp. 867–880, 1997.
[45] S. Rush and D. A. Driscoll, "Current distribution in the brain from surface electrodes," Anesth. Analg., vol. 47, no. 6, pp. 717–723, 1968.
[46] H. McCann, G. Pisano, and L. Beltrachini, "Variation in reported human head tissue electrical conductivity values," Brain Topogr., vol. 32, pp. 825–858, 2019.
[47] H. Helmholtz, "Ueber einige Gesetze der Vertheilung elektrischer Ströme in körperlichen Leitern mit Anwendung auf die thierisch-elektrischen Versuche" [Part I], Ann. Phys. Chem. (Poggendorff), vol. 89, pp. 211–233, 1853.
[48] H. Helmholtz, ibid. [Part II, "Schluss"], pp. 353–377, 1853.
[49] H. Helmholtz, "Messungen über den zeitlichen Verlauf der Zuckung animalischer Muskeln und die Fortpflanzungsgeschwindigkeit der Reizung in den Nerven," Arch. Anat. Physiol. wiss. Med. (Müller's Archiv), pp. 276–364, 1850.
[50] R. Plonsey, "Reciprocity applied to volume conductors and the ECG," IEEE Trans. Bio-Med. Electron., vol. BME-10, no. 1, pp. 9–12, 1963.
[51] R. Plonsey, Bioelectric Phenomena. New York: McGraw-Hill, 1969.
[52] J. Malmivuo and R. Plonsey, Bioelectromagnetism. Oxford Univ. Press, 1995, Ch. 11.
[53] M. Fernández-Corazza, S. Turovets, P. Luu, E. Anderson, and D. Tucker, "Transcranial electrical neuromodulation based on the reciprocity principle," Front. Psychiatry, vol. 7, art. 87, 2016.
[54] J. P. Dmochowski, A. Datta, M. Bikson, Y. Su, and L. C. Parra, "Optimized multi-electrode stimulation increases focality and intensity at target," J. Neural Eng., vol. 8, no. 4, art. 046011, 2011.
[55] J. P. Dmochowski, L. Koessler, A. M. Norcia, M. Bikson, and L. C. Parra, "Optimal use of EEG recordings to target active brain areas with transcranial electrical stimulation," NeuroImage, vol. 157, pp. 69–80, 2017.
[56] S. Wagner et al., "Using reciprocity for relating the simulation of transcranial current stimulation to the EEG forward problem," NeuroImage, vol. 140, pp. 163–173, 2016.

References

[57] S. Ogawa, T. M. Lee, A. R. Kay, and D. W. Tank, "Brain magnetic resonance imaging with contrast dependent on blood oxygenation," PNAS, vol. 87, no. 24, pp. 9868–9872, 1990.
[58] S. Ogawa et al., "Intrinsic signal changes accompanying sensory stimulation," PNAS, vol. 89, no. 13, pp. 5951–5955, 1992.
[59] R. B. Buxton, E. C. Wong, and L. R. Frank, "Dynamics of blood flow and oxygenation changes during brain activation: the balloon model," Magn. Reson. Med., vol. 39, no. 6, pp. 855–864, 1998.
[60] K. J. Friston, A. Mechelli, R. Turner, and C. J. Price, "Nonlinear responses in fMRI: the balloon model, Volterra kernels, and other hemodynamics," NeuroImage, vol. 12, no. 4, pp. 466–477, 2000.
[61] N. K. Logothetis, J. Pauls, M. Augath, T. Trinath, and A. Oeltermann, "Neurophysiological investigation of the basis of the fMRI signal," Nature, vol. 412, no. 6843, pp. 150–157, 2001.
[62] N. K. Logothetis, "What we can do and what we cannot do with fMRI," Nature, vol. 453, no. 7197, pp. 869–878, 2008.
[63] J. L. Parker, D. M. Karantonis, P. S. Single, M. Obradovic, and M. J. Cousins, "Compound action potentials recorded in the human spinal cord during neurostimulation for pain relief," Pain, vol. 153, no. 3, pp. 593–601, 2012.
[64] N. Mekhail et al., "Long-term safety and efficacy of closed-loop spinal cord stimulation to treat chronic back and leg pain (Evoke): a double-blind, randomised, controlled trial," Lancet Neurol., vol. 19, no. 2, pp. 123–134, 2020.
[65] N. Mekhail et al., "Durability of clinical and quality-of-life outcomes of closed-loop SCS for chronic back and leg pain: a secondary analysis of the Evoke RCT," JAMA Neurol., vol. 79, no. 3, pp. 251–260, 2022.
[66] N. Mekhail et al., "Long-term safety and efficacy of closed-loop SCS in patients with chronic pain: 36-month results," Reg. Anesth. Pain Med., vol. 49, no. 5, 2024 (online 2023).
[67] M. Russo et al., "Sustained long-term outcomes with closed-loop SCS: 12-month results of the prospective, multicenter, open-label Avalon study," Neurosurgery, vol. 87, no. 4, pp. E485–E495, 2020.
[68] C. R. Butson, S. E. Cooper, J. M. Henderson, and C. C. McIntyre, "Patient-specific analysis of the volume of tissue activated during deep brain stimulation," NeuroImage, vol. 34, no. 2, pp. 661–670, 2007.
[69] R. Polanía, M. A. Nitsche, and C. C. Ruff, "Studying and modifying brain function with non-invasive brain stimulation," Nat. Neurosci., vol. 21, no. 2, pp. 174–187, 2018.
[70] T. O. Bergmann and G. Hartwigsen, "Inferring causality from noninvasive brain stimulation in cognitive neuroscience," J. Cogn. Neurosci., vol. 33, no. 2, pp. 195–225, 2021.
[71] F. Karimi, M. Steiner, T. Newton, B. A. Lloyd, A. M. Cassarà, P. de Fontenay, S. Farcito, J. P. Triebkorn, E. Beanato, H. Wang, E. Iavarone, F. C. Hummel, N. Kuster, V. Jirsa, and E. Neufeld, "Precision non-invasive brain stimulation: an in silico pipeline for personalized control of brain dynamics," J. Neural Eng., vol. 22, no. 2, art. 026061, 2025.
[72] S. L. Metzger et al., "A high-performance neuroprosthesis for speech decoding and avatar control," Nature, vol. 620, no. 7976, pp. 1037–1046, 2023. [Author Correction: Nature 631:E13, 2024.]
[73] L. R. Hochberg et al., "Neuronal ensemble control of prosthetic devices by a human with tetraplegia," Nature, vol. 442, no. 7099, pp. 164–171, 2006.
[74] D. A. Moses et al., "Neuroprosthesis for decoding speech in a paralyzed person with anarthria," N. Engl. J. Med., vol. 385, no. 3, pp. 217–227, 2021.
[75] F. R. Willett, D. T. Avansino, L. R. Hochberg, J. M. Henderson, and K. V. Shenoy, "High-performance brain-to-text communication via handwriting," Nature, vol. 593, no. 7858, pp. 249–254, 2021.
Of course — here it is in your IEEE style:
[76] J. J. Tharayil, C. Zinno, F. Agnesi, B. Lloyd, S. Farcito, A. Cassarà, N. Kuster, M. Reimann, S. Micera, and E. Neufeld, "Simulation insights on the compound action potential in multifascicular nerves," *PLoS Comput. Biol.*, vol. 21, no. 9, art. e1013452, Sept. 2025. doi: 10.1371/journal.pcbi.1013452.
[77] McNeal, D. R. (1976). "Analysis of a Model for Excitation of Myelinated Nerve". IEEE Transactions on Biomedical Engineering. BME-23 (4): 329–337. doi:10.1109/TBME.1976.324593. PMID 1278925. S2CID 22334434.
[78] McIntyre et al (2002). J Neurophysiol. 87(2): 995–1006